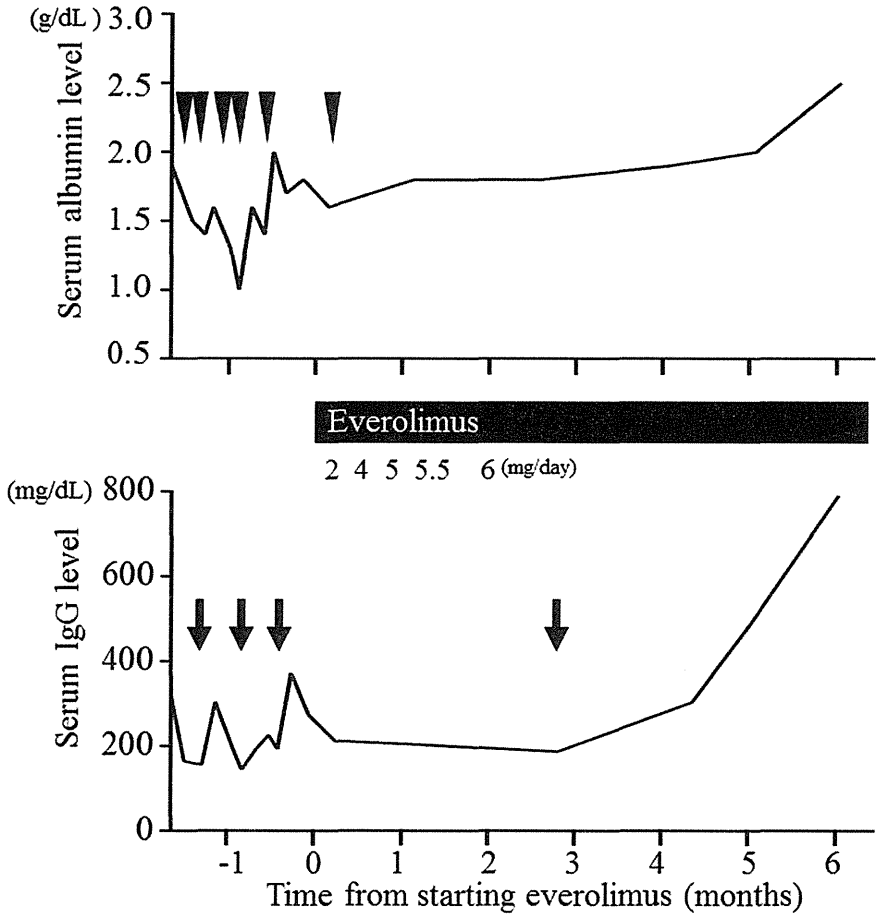

FIGURE 3
Serum albumin and IgG levels in relation to everolimus therapy in the patient. Inverted triangle indicates intravenous albumin infusion (12.5 g). Downward-pointing arrow indicates intravenous immunoglobulin infusion (5.0 g). Horizontal axis indicates time from the start of everolimus therapy.

are not well understood, although increased pressure in the lymph channels has been suggested as a possible cause.[14] Lymphatic hypoplasia results in obstruction of lymph flow, which leads to increased pressure within the lymphatics. This, in turn, causes dilation of the lymphatic channels in the intestine and leads to rupture of the channels with resultant loss of lymph into the bowel lumen.[15] Lymphangiography is a valuable tool for the detection of lymphatic leakage. Recently published reports indicate that lymphangiography plays a therapeutic role in patients with lymphatic leakage.[16] In our case, although lymphangiography was not performed, scintigraphy and α-1-antitrypsin clearance showed lymphatic leakage and obvious improvement with treatment. However, there were no changes in the enteroscopic findings after treatment. Everolimus might have effects on the function of the lymphatic canals, but no apparent effects on endoscopic findings.

Everolimus has been approved for use in Japan as an immunosuppressant for the prevention of cardiac and renal allograft rejection.[17] Practical experience has revealed that everolimus has some benefits over sirolimus. Although both substances are fairly similar chemically, the serum half-life of everolimus is shorter than that of sirolimus (28 vs 62 hours, respectively). Everolimus is more controllable because it reaches steady state earlier than does sirolimus (4 vs 6 days, respectively).[18] Additionally, everolimus is reportedly associated with a lower incidence of hyperlipidemia.[19] Although serious side effects are rare, it is necessary to monitor for their occurrence with any mTOR inhibitor therapy.

CONCLUSIONS

To the best of our knowledge, this is the first report of everolimus use in a patient with PIL. The clinical response to mTOR inhibitors such as sirolimus and everolimus may be related to inhibition of lymphatic endothelial cell growth and improvement in lymphatic canal function. Prospective studies are needed to determine the best systemic therapies for PIL with PLE and the optimal duration of treatment.

ACKNOWLEDGMENTS

We thank Dr Chiemi Saigo of Gifu University, Dr Hideki Matsumoto of Gifu Prefectural General Medical Center, and Drs Emi Kadoi and Kunihiro Shinoda of Gifu Municipal Hospital for their helpful comments. We also thank MT Yasuo Katagiri and MT Atsushi Nakagawa of Gifu University for technical assistance and the Department of Pediatrics at Gifu University for their contributions.

ABBREVIATIONS

mTOR: mammalian target of rapamycin
PIL: primary intestinal lymphangiectasia
PLE: protein-losing enteropathy
^{99m}Tc-has: ^{99m}Tc human serum albumin

the Ministry of Education, Culture, Sports, Science and Technology of Japan; Health and Labour Science Research Grants for Research on Intractable Diseases from the Ministry of Health, Labour and Welfare of Japan received by M.O.; and the Practical Research Project for Rare/Intractable Diseases from Japan's Agency for Medical Research and Development, AMED (15Aek0109057h0102).

POTENTIAL CONFLICT OF INTEREST: The authors have indicated they have no potential conflicts of interest to disclose.

REFERENCES

1. Trenor CC III, Chaudry G. Complex lymphatic anomalies. *Semin Pediatr Surg.* 2014;23(4):186–190
2. International Society for the Study of Vascular Anomalies. ISSVA classification for vascular anomalies. Available at: www.issva.org. Accessed May 2, 2015
3. Malone LJ, Fenton LZ, Weinman JP, Anagnost MR, Browne LP. Pediatric lymphangiectasia: an imaging spectrum. *Pediatr Radiol.* 2015;45(4):562–569
4. Vignes S, Bellanger J. Primary intestinal lymphangiectasia (Waldmann's disease). *Orphanet J Rare Dis.* 2008;3(5). Available at: www.ojrd.com/content/3/1/5
5. Binder HJ. Disorders of absorption. In: Brawnwald E, Fauci AS, Kasper DL, Hauser SL, Longo DL, Jameson JL, eds. *Harrison's principles of internal medicine,* 15th ed. New York: McGraw Hill; 2001:1665–1679
6. Kuroiwa G, Takayama T, Sato Y, et al. Primary intestinal lymphangiectasia successfully treated with octreotide. *J Gastroenterol.* 2001;36(2):129–132
7. Hammill AM, Wentzel M, Gupta A, et al. Sirolimus for the treatment of complicated vascular anomalies in children. *Pediatr Blood Cancer.* 2011;57(6):1018–1024
8. Lackner H, Karastaneva A, Schwinger W, et al. Sirolimus for the treatment of children with various complicated vascular anomalies. *Eur J Pediatr.* 2015;174(12):1579–1584
9. Persić M, Browse NL, Prpić I. Intestinal lymphangiectasia and protein losing enteropathy responding to small bowel restriction [letter]. *Arch Dis Child.* 1998;78(2):194
10. Ozeki M, Kanda K, Kawamoto N, et al. Propranolol as an alternative treatment option for pediatric lymphatic malformation. *Tohoku J Exp Med.* 2013;229(1):61–66
11. Ozeki M, Fukao T, Kondo N. Propranolol for intractable diffuse lymphangiomatosis. *N Engl J Med.* 2011;364(14):1380–1382
12. Vignot S, Faivre S, Aguirre D, Raymond E. mTOR-targeted therapy of cancer with rapamycin derivatives. *Ann Oncol.* 2005;16(4):525–537
13. Hokari R, Kitagawa N, Watanabe C, et al. Changes in regulatory molecules for lymphangiogenesis in intestinal lymphangiectasia with enteric protein loss. *J Gastroenterol Hepatol.* 2008;23(7 Pt 2):e88–e95
14. Mistilis SP, Skyring AP, Stephen DD. Intestinal lymphangiectasia. Mechanism of enteric loss of plasma-protein and fat. *Lancet.* 1965;1(7376):77–79
15. Toskes P. Gastrointestinal diseases: malabsorption. In: Wyngaarden J, Smith L, eds. *Cecil Textbook of Medicine,* 18th ed. Philadelphia: WB Saunders; 1988:732–745
16. Matsumoto T, Yamagami T, Kato T, et al. The effectiveness of lymphangiography as a treatment method for various chyle leakages. *Br J Radiol.* 2009;82(976):286–290
17. Chapman TM, Perry CM. Everolimus. *Drugs.* 2004;64(8):861–872, discussion 873–874
18. Pascual J, Boletis IN, Campistol JM. Everolimus (Certican) in renal transplantation: A review of clinical trial data, current usage and future directions. *Transplant Rev.* 2006;20(1):1–18
19. Tenderich G, Fuchs U, Zittermann A, Muckelbauer R, Berthold HK, Koerfer R. Comparison of sirolimus and everolimus in their effects on blood lipid profiles and haematological parameters in heart transplant recipients. *Clin Transplant.* 2007;21(4):536–543

Clinical Features and Prognosis of Generalized Lymphatic Anomaly, Kaposiform Lymphangiomatosis, and Gorham–Stout Disease

Michio Ozeki, MD, PhD,[1]* Akihiro Fujino, MD, PhD,[2] Kentaro Matsuoka, MD, PhD,[3] Shunsuke Nosaka, MD, PhD,[4] Tatsuo Kuroda, MD, PhD,[2] and Toshiyuki Fukao, MD, PhD[1]

Background. Complex lymphatic anomalies are intractable lymphatic disorders, including generalized lymphatic anomaly (GLA), Gorham–Stout disease (GSD), and kaposiform lymphangiomatosis (KLA). The etiology of these diseases remains unknown and diagnosis is confused by their similar clinical findings. This study aimed to clarify the differences in clinical features and prognosis among GLA, KLA, and GSD, in Japanese patients. ***Procedure.*** Clinical features, radiological and pathological findings, treatment, and prognosis of patients were obtained from a questionnaire sent to 39 Japanese hospitals. We divided the patients into three groups according to radiological findings of bone lesions and pathology. Differences in clinical findings and prognosis were analyzed. ***Results.*** Eighty-five patients were registered: 35 GLA, 9 KLA, and 41 GSD. Disease onset was more common in the first two decades of life (69 cases). In GSD, osteolytic lesions were progressive and consecutive. In GLA and KLA, 18 patients had osteolytic lesions that were multifocal and nonprogressive osteolysis. Thoracic symptoms, splenic involvement, and ascites were more frequent in GLA and KLA than in GSD. Hemorrhagic pericardial and pleural effusions were more frequent in KLA than GLA. GSD had a significantly favorable outcome compared with combined GLA and KLA ($P = 0.0005$). KLA had a significantly poorer outcome than GLA ($P = 0.0268$). ***Conclusions.*** This survey revealed the clinical features and prognosis of patients with GLA, KLA, and GSD. Early diagnosis and treatment of KLA are crucial because KLA has high mortality. Further prospective studies to risk-stratify complex lymphatic anomalies and optimize management for KLA are urgently needed. Pediatr Blood Cancer

Key words: complex lymphatic anomaly; generalized lymphatic anomaly; Gorham–Stout disease; kaposiform lymphangiomatosis; lymphatic malformation; osteolysis

INTRODUCTION

Complex lymphatic anomaly is a recently proposed disease category of intractable lymphatic disorders, including generalized lymphatic anomaly (GLA) and Gorham–Stout disease (GSD).[1] The current literature is confined to case reports and several small series because of the low incidence of these diseases. The clinical features and mortality rate of the patients remain unknown. In some patients, proper diagnosis is difficult because the clinical findings are overlapping.

GLA is characterized by diffuse or multicentric proliferation of dilated lymphatic vessels resembling common lymphatic malformation (LM). The International Society for the Study of Vascular Anomalies (ISSVA) has recently suggested replacing the term "lymphangiomatosis" with GLA. This is because the suffix "oma" implies neoplastic proliferation.[2] GLA may present at birth but may also occur in children and young adults. It has a variable presentation and can affect several different sites including bone, liver, spleen, mediastinum, lungs, and soft tissues. The clinical course is directly related to the affected sites and extent of the disease.[3] Thoracic involvement may be associated with poor prognosis compared with cases with soft tissue or bone involvement.[4]

GSD is a rare disease characterized by osteolysis in bony segments, with localized proliferation of lymphatic or vascular channels in areas adjacent to the affected bone.[5] Several bones may become involved and these undergo progressive destruction and resorption. Areas commonly affected by GSD include ribs, cranium, clavicle, and cervical spine.[6] Pain and swelling in the affected area may occur. While GSD mainly involves the skeletal system, it can also involve the viscera, and clinical findings of GSD and GLA closely overlap.[7] Lala et al. have reported that patients with GLA and GSD displayed differences in the radiological findings of their bone lesions; GLA patients have lytic areas confined to the medullary cavity, whereas GSD patients have progressive osteolysis resulting in the loss of cortical bone.[6] Although these diseases are known as different conditions, affected bones from both groups of patients show abnormal lymphatic channels and appear histologically similar. Further study of GLA and GSD will help delineate the clinical,

Additional Supporting Information may be found in the online version of this article.

Abbreviations: CT, computed tomography; GLA, generalized lymphatic anomaly; GSD, Gorham–Stout disease; ISSVA, International Society for the Study of Vascular Anomalies; KLA, kaposiform lymphangiomatosis; LM, lymphatic malformation; MRI, magnetic resonance imaging

[1]Department of Pediatrics, Graduate School of Medicine, Gifu University, Gifu, Japan; [2]Department of Pediatric Surgery, Keio University School of Medicine, Tokyo, Japan; [3]Department of Pathology, National Center for Child Health and Development, Tokyo, Japan; [4]Department of Radiology, National Center for Child Health and Development, Tokyo, Japan

Grant sponsor: National Center for Child Health and Development (24-19); Grant sponsor: Grant-in-Aid for Scientific Research from the Ministry of Education, Culture, Sports, Science and Technology of Japan; Grant number: 25461587; Grant sponsor: Health and Labour Science Research Grant for Research on Intractable Diseases from the Ministry of Health, Labour and Welfare of Japan; Grant sponsor: Practical Research Project for Rare/Intractable Diseases from Japan's Agency for Medical Research and Development, AMED; Grant number: 15Aek0109057h0102.

Conflict of interest: Nothing to declare.

*Correspondence to: Michio Ozeki, Department of Pediatrics, Graduate School of Medicine, Gifu University, 1-1 Yanagido, Gifu 501-1194, Japan. E-mail: michioo@gifu-u.ac.jp

Received 20 August 2015; Accepted 30 December 2015

DOI 10.1002/pbc.25914
Published online in Wiley Online Library (wileyonlinelibrary.com).

histological, and genetic similarities and differences between these two rare diseases.

Kaposiform lymphangiomatosis (KLA) has recently been distinguished as a novel subtype of GLA with foci of spindle endothelial cells amid a background of malformed lymphatic channels.[8] All cases of KLA involve multiple organs with a predilection for the thoracic cavity, causing pleural effusion that commonly leads to respiratory distress and dyspnea.

The etiology of these diseases is poorly understood and it is likely that the diseases represent a clinical spectrum of lymphatic pathological processes. However, recent studies about this spectrum of lymphatic diseases have suggested differences in the clinical characteristics of these complex lymphatic anomalies. The purposes of the present study were to investigate the clinical features of patients with these diseases, and to clarify the differences among the diseases and their prognoses.

METHODS

Ethical Approval, Organization, Questionnaire, and Data Collection

The Institutional Review Board of Gifu University Graduate School of Medicine approved this study. To elucidate the clinical characteristics of GLA and GSD, we conducted a nationwide, questionnaire-based survey in Japan under the auspices of the Japanese Ministry of Health, Labour and Welfare Research Program into Intractable Diseases Research Grants. The first set of questionnaires was sent to 520 Japanese hospitals with pediatric departments. The first questionnaire queried how many patients with GLA and GSD the target hospitals had between 2000 and 2013. We did not ask about KLA because it was not a known disease at the start of the study. The second set of questionnaires, which focused on clinical information such as age at onset and diagnosis, family history, perinatal history, symptoms, lesion site, radiographic and pathological findings, treatment, complications, clinical course, and outcome of patients, was sent to their attending physicians. Additionally, we requested that the authors, who had reported GLA and GSD in the literature in the past 10 years, complete the second questionnaire. To avoid reporting duplicate data, we identified overlapping patients by date of birth, sex, home village, and time of diagnosis.

Data Curation, Review of Pathological and Radiological Examinations, and Diagnosis

We categorized collected patients into GLA, KLA, and GSD according to pathological and radiological examinations. Exclusion criteria included diagnosis of other lymphatic diseases, for example, localized common LM lesions without extensive involvement, central conductive lymphatic anomaly, and lymphedema, or insufficient data. The pathological examinations were reviewed retrospectively. We defined as KLA foci of spindle endothelial cells amid a background of malformed lymphatic channels.[8] As noted previously, the key features of GSD are osteolysis and disappearing bone.[9] To diagnose GSD, the radiological findings of all patients were reviewed. Thus, only patients with evidence of cortical loss and/or progressive bone resorption were categorized as having GSD.[6] Patients with evidence of lytic bone confined to the medullary cavity or without bone lesions were diagnosed with GLA. Clinical data of these patients were carefully reviewed by two pediatric specialists (T.H. and K.K.). Pathological examinations were reviewed independently by a pediatric pathologist (K.M.). Imaging examinations were reviewed independently by a pediatric radiologist (S.N.). In cases of diagnostic discrepancy, a final decision was reached by consensus.

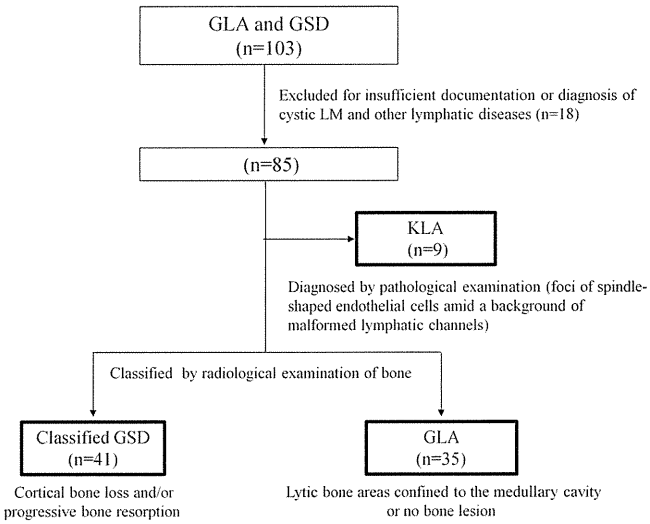

Fig. 1. Diagnostic charts of GLA, KLA, and GSD. GLA, generalized lymphatic anomaly; GSD, Gorham–Stout disease; KLA, kaposiform lymphangiomatosis.

Data Analysis

Because of the similarity between GLA and KLA, the findings including the number and distribution of bones involved in these two groups combined were initially compared with GSD, and then specific differences between GLA and KLA were sought. Prognosis as measured by overall survival was compared in the same way.

Statistical analysis was performed with GraphPad Prism version 6. Descriptive statistical methods (median and standard deviation), Wilcoxon's rank sum test for comparison of age, the number of bones involved, duration from symptom onset to diagnosis and follow-up period, and Fisher's exact test for two-group comparison, were used for the statistical analyses. Overall survival was analyzed from the date of onset by the product–sum method of Kaplan–Meier. The differences in survival times between the combined GLA and KLA group and GSD group, or GLA group and KLA group, were compared with the log-rank test. A value of $P < 0.05$ was considered statistically significant.

RESULTS

Patients and General Characteristics at Study Entry

A total of 420 responses (80.7% response rate) were received to the first set of questionnaires. A second questionnaire was then sent to 39 institutions, asking for information regarding clinical features, treatments, and outcomes for each patient. One hundred and three patients were diagnosed with GLA and GSD.

Eighteen cases were excluded because of insufficient documentation or diagnosis of other lymphatic diseases. Therefore, 85 patients were included in our study. Pathological examination was available in 71 patients (83.5%). It was not available in 14 patients because of the following reasons: examination was not performed (n = 6), pathological specimens were already disposed or for internal hospital use only (n = 4), or we could not obtain the cooperation of the primary doctor (n = 4). We categorized these patients into GLA or GSD according to pathological diagnosis in the survey center and radiological examinations. The number of patients with GSD, GLA, and KLA was 41, 35, and 9, respectively (Fig. 1). Among 44 patients with GLA and KLA, 39 (88.6%) underwent pathological examination for confirmation of diagnosis. Two patients did not undergo pathological examination because they died from rapid progression of respiratory failure. These two patients also had severe thrombocytopenia and coagulation disorder at clinical diagnosis. Another three patients without pathological examination were all infants (0, 7, and 12 months old) and their diagnosis was made by radiological examination alone.

The clinical characteristics of the patients are shown in Supplemental Table I. No family and perinatal history was evident for any of these patients. There was no significant difference in the male-to-female ratio among the three groups of patients. The median age of all patients at the time of data collection was 19.0 years (range: 1.3–70 years). The median ages of the GLA, KLA, and GSD groups were 18.0 (range: 1.3–70), 10.0 (range: 1.5–18.5), and 21.9 (range: 1.5–64.7) years, respectively. Age of onset ranged from infancy to adulthood (mean: 12.0, range: 0–63 years) but disease was more common in the first two decades of life (69/85, 81.2%), and 18 patients were aged <1 year, most of whom (12 infants) had GLA. The duration between onset and diagnosis in the three groups did not differ significantly. However, the duration in the KLA patients tended to be shorter than in other groups.

Characteristics of Affected Areas

Bone lesions, being a diagnostic criterion, were present in all patients diagnosed with GSD, but were also present in 40.9% (18 of 44) of GLA or KLA patients (Supplemental Table II). Osteolysis was the most common finding. The typical bone resorption in GSD is shown in Figures 2A, 2C, and 2D. In GLA and KLA, 16 of 44 (36.4%) patients had osteolysis, which was characterized by multiple lytic changes (Figs. 3A–3C). There were no significant radiological differences in the bone lesions between GLA and KLA. In GSD, pathological fracture was more frequent. A greater number of bones were involved in GLA or KLA than in GSD (Supplemental Table III). The spine was the most common site of osseous changes in all patients, and the spine lesions were identified more often in GLA or KLA than GSD (Fig. 3C). In GSD, 19 patients (54.3%) had bone lesions in any of the four limbs (14 femur, four humerus, nine lower leg, and two tarsal bone). With regard to skeletal axis of the osteolytic lesion, the axial skeleton (skull, spine, and ribs) was affected in 16 of the 18 patients with GLA or KLA. However, the appendicular skeleton (scapula, clavicle, pelvis, ilium, and four limbs) was only affected in six patients. An infiltrative soft tissue abnormality adjacent to the area of osseous involvement was identified more often in GSD than GLA or KLA ($P \leq 0.001$).

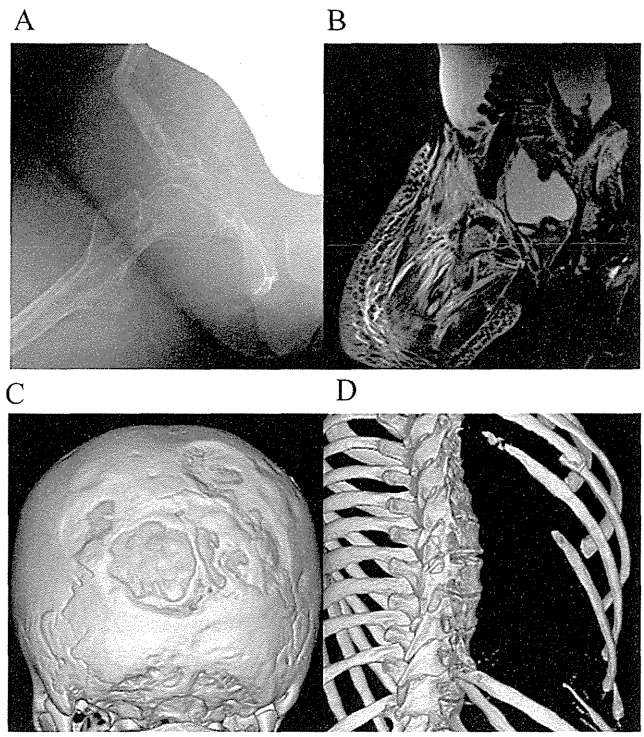

Fig. 2. Radiological findings of patients with GSD. (**A** and **B**) Thirteen-year-old female with GSD involving right lower extremity, right pelvis, spine, abdomen, and right thorax. (**A**) Plain radiograph of the right pelvis shows osteolysis at the proximal femoral shaft as well as the pelvic bone. (**B**) Coronal fat suppressed in T2-weighted image of the pelvis demonstrates extensive high signal intensity in the soft tissue surrounding the femur as well as subcutaneous fat tissue. Involved right pelvis shows high signal intensity secondary to osteolysis. Also visible is a large amount of ascites. (**C**) Nine-year-old male with GSD involving the occipital and temporal bones. Posterior view of 3D CT imaging shows almost complete resorption of the occipital bone. (**D**) Thirteen-year-old female with GSD involving the ribs. Right oblique posterior view of 3D CT shows multiple osteolysis and fracture of the posterior portion of the right 5–10 ribs. CT, computed tomography; GSD, Gorham–Stout disease (GSD).

Thoracic lesions were the second most common, with symptoms of cough, chest pain, dyspnea, and wheezing. Some patients experienced wheezing and were misdiagnosed with asthma prior to recognition of the lymphatic disorder. Pleural effusion, mediastinal mass, and cardiac effusion were significantly more frequent in GLA and KLA than GSD ($P = 0.002$, 0.002, and 0.001, respectively). The frequency of pleural and cardiac effusion in KLA was similar to that in GLA, but mediastinal masses and hemorrhagic pericardial and pleural effusions were more frequent in KLA than GLA ($P = 0.017$ and <0.001, respectively). The other findings were heart failure, cardiac tamponade, and pulmonary infiltration and hemorrhage. In abdominal lesions, splenic involvement and ascites were more frequent in GLA and KLA than GSD ($P = 0.044$ and 0.001, respectively). However, KLA patients did not have ascites. Seven patients had cystic LM of the mesentery and retroperitoneum, in combination with ascites or invasion of the surrounding soft tissue. Skin lesions were present in 36 of 85 (42.3%) cases. Three patients

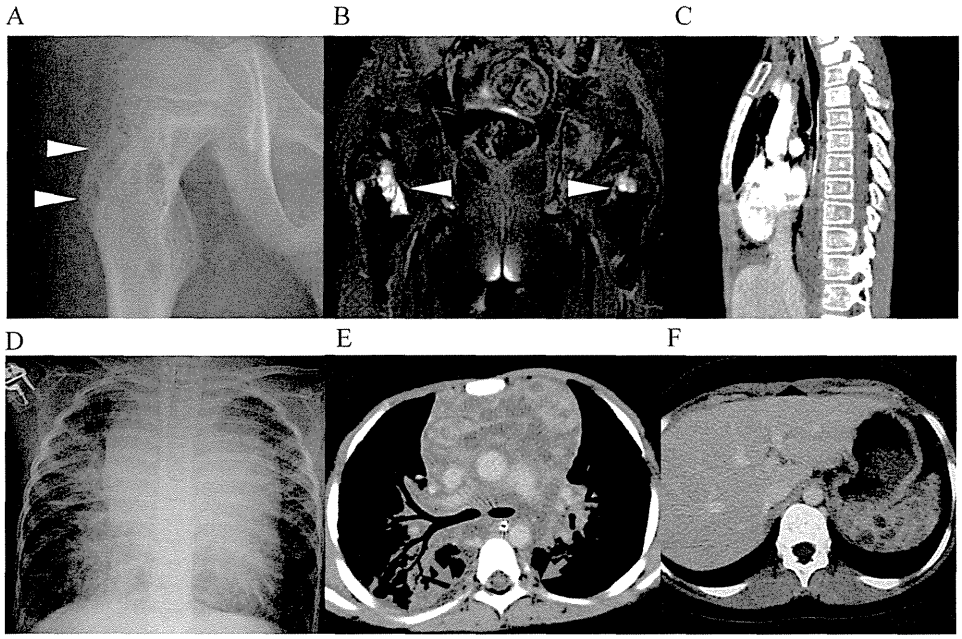

Fig. 3. Radiological findings of patients with GLA and KLA. (**A–C** and **F**) Twelve-year-old male with GLA involving bone and spleen. (**A**) Plain radiography of femoral head shows a small lytic lesion (white arrowheads). (**B**) Coronal fat suppressed, T2-weighted MRI of femoral head shows a small lytic lesion (white arrowheads). (**C**) Contrast-enhanced CT of the chest with sagittal reconstruction shows dissemination of osteolysis in the vertebrae. (**D** and **E**) Eight-year-old male with KLA involving the thoracic region. (**D**) Chest radiography shows pronounced effusion, mediastinal enlargement, and peribronchovascular infiltration extending from the hilar to the peripheral area. (**E**) Chest contrast-enhanced CT demonstrates diffuse thickening of the interlobular septa, pleural effusion in the right lung, and retroperitoneal soft tissue mass (red arrows). (**F**) An axial projection shows multiple cystic lesions in the spleen. CT, computed tomography; GLA, generalized lymphatic anomaly; KLA, kaposiform lymphangiomatosis; MRI, magnetic resonance imaging.

had subcutaneous macrocytic LMs at birth. Neurological disorders were uncommon (10/85 [11.8%]) and were associated with osteolytic lesions of the skull.

Imaging and Histopathological Examination

Bone lesions were present in 59 of 85 cases and imaging examinations of bone lesions included plain radiography (n = 59), computed tomography ([CT]; n = 59), magnetic resonance imaging ([MRI]; n = 57), and bone scintigraphy (n = 3). CT showed more definite location and number of osteolytic lesions than did plain radiography. MRI demonstrated altered signaling in bone marrow, which was hypointense on T1-weighted imaging. An infiltrative soft tissue abnormality adjacent to the area of osseous involvement was characterized by high signal intensity in T2-weighted imaging, which indicated lymphatic infiltration or accumulation of lymphatic fluid (Fig. 2B). Bone scintigraphy demonstrated increased uptake of radiotracer in the pathological fracture of one case, while there was no increased uptake in the osteolytic lesion. In thoracic lesions of typical patients with GLA or KLA, bilateral interstitial infiltrates in the lung and pericardial or pleural effusions were evident on chest radiography (Fig. 3D). Thoracic CT revealed diffuse smooth thickening of interlobular septa and bronchovascular bundles, with extensive involvement of mediastinal connective tissue and perihilar regions. The thickening and soft tissue mass of the pleura, posterior mediastinum, and anterior ribs were characteristic findings, especially in KLA (Fig. 3E). Thirty-three patients had splenic involvement, identified by CT (n = 33), MRI (n = 29), and ultrasound (n = 20). These lesions were multiple cystic lesions in most cases (Fig. 3F). On Doppler ultrasound, the lesions did not demonstrate increased vascular flow. Histopathology demonstrated anastomosing endothelium-lined spaces consistent with lymphatic vessels stained with D2-40 (Figs. 4A–4F). Although KLA was diagnosable by characteristic findings at pathological examination, there were no significant histopathological differences between GLA and GSD. Bone biopsy specimens showed dilated lymphatic lumens containing lymphatic fluid in lytic lesions; however, some specimens were not in sufficiently good condition to reconstruct their architecture for diagnosis.

Treatments

Treatment included medication, surgery, radiotherapy, and nutritional therapy. In patients with bone lesions, medical treatment included interferon-α, propranolol, bisphosphonates, and corticosteroids. When these medications were not effective, patients needed to undergo surgery or symptomatic treatment. Surgical interventions included resection of the lesion and orthopedic operations (fracture reduction or reconstruction). In some patients, surgical reconstruction undertaken to control the disease was unsuccessful because of rapid osteolysis and resorption of bone graft material. The common surgical procedures for pleural effusion were pleurocentesis, pleurodesis, and ligation of the thoracic duct. Medical therapy for thoracic lesions included corticosteroids, propranolol, interferon-α, octreotide, and mammalian target of rapamycin (mTOR) inhibitor. Sixteen patients

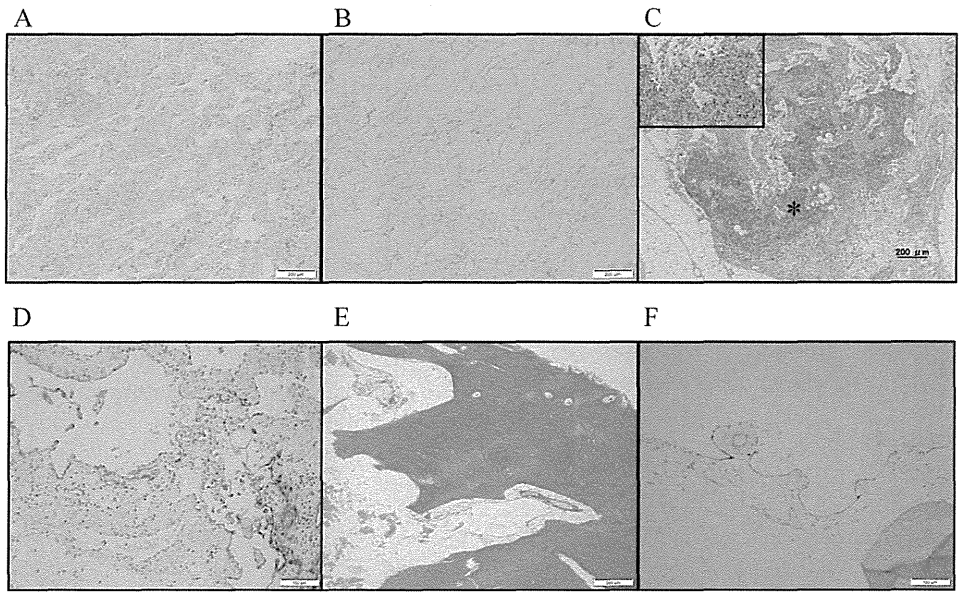

Fig. 4. Pathological findings in patients with GLA, KLA, and GSD. (**A** and **B**) Specimen of subcutaneous lesion from GLA patient. (**A**) This specimen shows proliferation of thin-walled, anastomosing lymphatic vessels lined by a single layer of endothelial cells without foci of spindle endothelial cells (bar 200 μm, hematoxylin and eosin [H&E]). (**B**) Endothelial cells were identified as lymphatic using D2-40 (bar 100 μm). (**C** and **D**) Specimen of thoracic lesion from KLA patient. (**C**) Specimen shows proliferation of thin-walled, anastomosing lymphatic vessels lined by a single layer of endothelial cells with a focus of spindle cells (*) (bar 200 μm, H&E). Spindle cells can be seen in the insert image. (**D**) Endothelial cells were identified as lymphatics using D2-40 (bar 100 μm). (**E** and **F**) Specimen of femur biopsy affected by GSD. (**E**) Typical bone structures were resorbed and replaced by thin-walled endothelium-lined capillaries of vascular or lymphatic origin (bar 200 μm, H&E). (**F**) D2-40 immunostaining delineates the endothelium of lymphatic channels (bar 100 μm, H&E). GLA, generalized lymphatic anomaly; GSD, Gorham–Stout disease; KLA, kaposiform lymphangiomatosis.

(six with bone lesions of GSD, and 10 with thoracic lesions) underwent radiotherapy. The total doses applied and fractionation regimens varied widely among patients and lesions. Nutritional therapy (fat-restricted diet and low-fat medium chain triglyceride diet) had no effects in almost all patients.

Follow-up Period and Mortality

Follow-up was available for all patients. The mean follow-up period was 7.0 (range, 0.1–32; median, 4) years. Overall or in aggregate, mortality rate was 20% (17/85) and the cause of death was thoracic symptoms (Fig. 5A). All 29 patients (nine adults and 20 children) who lacked thoracic lesions survived. Of the 69 pediatric patients, 50 had thoracic lesions and 13 died (26%). The GSD group had a significantly more favorable outcome than the combined GLA and KLA group had ($P = 0.0005$) (Fig. 5B). In contrast, the KLA patients had a significantly poorer outcome than the GLA patients had ($P = 0.0268$) (Fig. 5C).

DISCUSSION

In this nationwide retrospective observational study, we collected data on follow-up of patients with GLA, KLA, or GSD from Japanese hospitals. This study demonstrated the frequency and features of principal symptoms, diagnostic signs, and prognosis. Our data contribute to understanding the clinical features and prognosis of these diseases.

Osteolytic lesions are important for differential diagnosis. They can be caused by several different conditions including infection, inflammation, cancer, and endocrine disorders. In our study, some cases were misdiagnosed as Langerhans cell histiocytosis and osteomyelitis before definitive diagnosis. There is no specific test or procedure to diagnose GSD definitively;[3] thus, diagnosis is based upon identification of characteristic symptoms, detailed patient history, radiological examination, and histopathological findings. Especially, radiological findings of osteolysis seem important to distinguish among GLA, KLA, and GSD. Patients with GLA and KLA displayed lytic areas confined to the medullary cavity, whereas patients with GSD showed progressive osteolysis resulting in the loss of cortical bone. GLA and KLA typically involved more bones than GSD did. The bone lesions of GSD were often progressive and sequentially infiltrative; in contrast, those of GLA and KLA were nonprogressive. However, our study also showed that there were some overlapping features and no obvious difference in bone histopathology.

KLA was recently distinguished as a novel subtype of GLA.[8,10] Although dilated malformed lymphatic channels lined by a single layer of endothelial cells are common to both GLA and KLA, the latter also has foci of patternless clusters of intra- or perilymphatic spindled cells associated with platelet microthrombi, extravasated red blood cells, hemosiderin, and some degree of fibrosis. Patients with KLA also have coagulation disorders, and hemorrhagic pericardial and pleural effusions.[8] In our study, nine patients were diagnosed pathologically with KLA from among those who were diagnosed with GLA. The multiple overlapping clinical characteristics and radiological findings of GLA have led to a hypothesis that KLA may arise from GLA. There have been no cases of

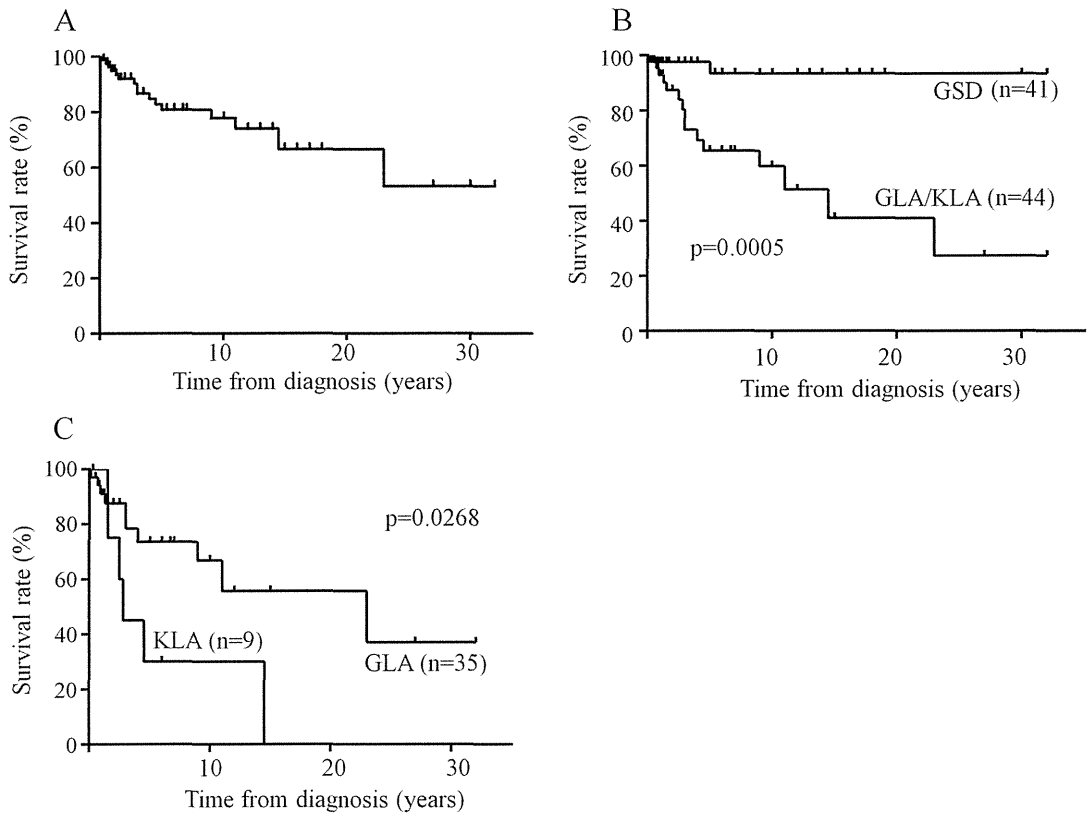

Fig. 5. Kaplan–Meier curve showing time from onset. (**A**) Overall survival of all cases (n = 85). (**B**) Overall survival in GSD group (n = 41) compared with combined GLA and KLA group (n = 44). The GSD group had a significantly more favorable outcome than the combined GLA and KLA group had ($P = 0.0005$) (**C**). Overall survival in GLA group (n = 35) compared with KLA group (n = 9). KLA group had a significantly poorer outcome than the GLA group had ($P = 0.0268$). GLA, generalized lymphatic anomaly; GSD, Gorham–Stout disease; KLA, kaposiform lymphangiomatosis.

GLA that have evolved into KLA over several months or years. However, patients with KLA had unfavorable prognosis and serious symptoms (hemorrhagic pericardial and pleural effusions). We might have to distinguish KLA from GLA or other LMs.

In patients with multifocal lesions, therapeutic options are palliative, and therapy is often aimed at reducing symptoms associated with bone lesions and chylous effusions.[11] Management of chylothorax is often the primary concern. Thoracentesis and pleural drainage are used to treat chylothorax to relieve respiratory distress. In the case of failure with such conservative treatment, thoracic duct ligation has been used to treat pleural effusion in isolated cases.[4] Radiotherapy has been used in cases in which surgery is not possible, or in combination with surgery. Several case reports have described the successful use of radiotherapy, achieving pain relief and arresting the spread of osteolysis. Positive results have been achieved with a total dose of 30–45 Gy.[11]

Patients with osteolysis have been treated with drugs that inhibit bone resorption, including bisphosphonates such as pamidronic or zoledronic acid.[12] Patients with bone or thoracic lesions have been treated with interferon-α-2b, which inhibits the formation of lymphatic vessels.[13] Other pharmaceuticals include vascular endothelial growth factor-A antibody, bevacizumab,[14] propranolol,[15] steroids, vitamin D, and calcitonin. These treatments, used alone or in combination, improve symptoms in some cases, but their effectiveness is inconsistent. A recent study suggested that the antilymphangiogenic properties of rapamycin (sirolimus; an mTOR inhibitor) and its derivatives might have therapeutic value for the prevention and treatment of malignancies.[16] In our study, there were nine patients (eight with thoracic and seven with bone lesions) who were treated with an mTOR inhibitor. Further investigation is needed to determine which treatments are effective and safe in these patients.

It is necessary to address the limitations and bias of the present study. This was a retrospective survey that was limited to general hospitals with pediatric departments and physicians who reported cases. There was also responder bias in that providers managing the most severe cases may have been more likely to report them. When we started this survey in 2013, a new classification of ISSVA had not been announced and there were no standard diagnostic criteria for complex lymphatic anomalies. Therefore, there was some possible involvement of other similar diseases. Multifocal lymphangioendotheliomatosis with thrombocytopenia, multifocal kaposiform hemangioendothelioma, and central conducting lymphatic anomalies are rare diseases, but could be misdiagnosed as GLA.[17,18] Patients diagnosed with GLA might have KLA because of a lack of characteristic findings at pathological examination. In

addition to the above limitations, it is probable that classification of vascular anomalies will be rationally modified according to advances in genetic and clinicopathological research in the future. Despite the above-mentioned limitations, this study is noteworthy because it was a large detailed survey of GLA, KLA, and GSD. We believe that sufficient data were collected to characterize the frequency of principal symptoms, diagnostic signs, and prognosis.

In conclusion, we performed a nationwide, questionnaire-based survey of complex lymphatic anomalies, GLA, GSD, and KLA, to characterize their prevalence, clinical features, radiological and pathological findings, treatment, and prognosis. This study revealed the clinical presentation and severe course of the patients, and limited current therapeutic options. Further study into the pathogenesis and a prospective study are needed for better therapy with improved outcome, especially for KLA.

ACKNOWLEDGMENTS

This study was supported by a grant from the National Center for Child Health and Development (24-19); Grant-in-Aid for Scientific Research from the Ministry of Education, Culture, Sports, Science and Technology of Japan (25461587); a Health and Labour Science Research Grant for Research on Intractable Diseases from the Ministry of Health, Labour and Welfare of Japan received by M.O.; and Practical Research Project for Rare/Intractable Diseases from Japan's Agency for Medical Research and Development, AMED (15Aek0109057h0102). We thank the cooperative institutions in Japan and Dr. Tomohiro Hori, Dr. Kaori Kanda, and Dr. Norio Kawamoto, Gifu University, for helpful comments and data review. We also thank the Department of Pediatrics at Gifu University for its contribution.

REFERENCES

1. Trenor CC 3rd, Chaudry G. Complex lymphatic anomalies. Semin Pediatr Surg 2014;23:186–190.
2. International society for the study of vascular anomalies: ISSVA classification for vascular anomalies (Approved at the 2-th ISSVA Workshop, Melbourne, April 2014). http://issva.org. Accessed April 2014.
3. Blei F. Lymphangiomatosis: Clinical overview. Lymphat Res Biol 2011;9:185–190.
4. Alvarez OA, Kjellin I, Zuppan CW. Thoracic lymphangiomatosis in a child. J Pediatr Hematol Oncol 2004;26:136–141.
5. Radhakrishnan K, Rockson SG. Gorham's disease: An osseous disease of lymphangiogenesis? Ann N Y Acad Sci 2008;1131:203–205.
6. Lala S, Mulliken JB, Alomari AI, Fishman SJ, Kozakewich HP, Chaudry G. Gorham–Stout disease and generalized lymphatic anomaly – Clinical, radiologic, and histologic differentiation. Skeletal Radiol 2013;42:917–924.
7. Michael TD, Nupur G, Bjorn RO. Viewpoints on vessels and vanishing bones in Gorham–Stout disease. Bone 2014;63:47–52.
8. Croteau SE, Kozakewich HP, Perez-Atayde AR, Fishman SJ, Alomari AI, Chaudry G4, Mulliken JB, Trenor CC 3rd. Kaposiform lymphangiomatosis: A distinct aggressive lymphatic anomaly. J Pediatr 2014;164:383–388.
9. Gorham LW, Stout AP. Massive osteolysis (acute spontaneous absorption of bone, phantom bone, disappearing bone); its relation to hemangiomatosis. J Bone Joint Surg Am 1955;37-A:985–1004.
10. Dasgupta R, Fishman SJ. ISSVA classification. Semin Pediatr Surg 2014;23:158–161.
11. Hagendoorn J, Yock TI, Borel Rinkes IH, Padera TP, Ebb DH. Novel molecular pathways in Gorham disease: Implications for treatment. Pediatr Blood Cancer 2014;61:401–406.
12. Heyd R, Micke O, Surholt C, Berger B, Martini C, Füller J, Schimpke T, Seegenschmiedt MH. German Cooperative Group on Radiotherapy for Benign Diseases (GCG-BD). Radiation therapy for Gorham–Stout syndrome: Results of a national patterns-of-care study and literature review. Int J Radiat Oncol Biol Phys 2011;81:179–185.
13. Kuriyama DK, McElligott SC, Glaser DW, Thompson KS. Treatment of Gorham–Stout disease with zoledronic acid and interferon-alpha: A case report and literature review. J Pediatr Hematol Oncol 2010;32:579–584.
14. Ozeki M, Funato M, Kanda K, Ito M, Teramoto T, Kaneko H, Fukao T, Kondo N. Clinical improvement of diffuse lymphangiomatosis with pegylated interferon alfa-2b therapy: Case report and review of the literature. Pediatr Hematol Oncol 2007;24:513–524.
15. Grunewald TG, Damke L, Maschan M, Petrova U, Surianinova O, Esipenko A, Konovalov D, Behrends U, Schiessl J, Wörtler K, Burdach S, von Luettichau I. First report of effective and feasible treatment of multifocal lymphangiomatosis (Gorham–Stout) with bevacizumab in a child. Ann Oncol 2010;21:1733–1734.
16. Ozeki M, Fukao T, Kondo N. Propranolol for intractable diffuse lymphangiomatosis. N Engl J Med 2011;364:1380–1382.
17. Reinglas J, Ramphal R, Bromwich M. The successful management of diffuse lymphangiomatosis using sirolimus: A case report. Laryngoscope 2011;121:1851–1854.
18. Nakaya T, Morita K, Kurata A, Ushiku T, Igarashi T, Kuroda M, Fukayama M. Multifocal kaposiform hemangioendothelioma in multiple visceral organs: An autopsy of 9-day-old female baby. Hum Pathol 2014;45:1773–1777.
19. Kline RM, Buck LM. Bevacizumab treatment in multifocal lymphangioendotheliomatosis with thrombocytopenia. Pediatr Blood Cancer 2009;52:534–536.

BRIEF REPORT
Gorham–Stout Disease of the Skull Base With Hearing Loss: Dramatic Recovery and Antiangiogenic Therapy

Akifumi Nozawa, MD,[1] Michio Ozeki, MD, PhD,[1]* Bunya Kuze, MD, PhD,[2] Takahiko Asano, MD, PhD,[3] Kentaro Matsuoka, MD, PhD,[4] and Toshiyuki Fukao, MD, PhD[1]

Gorham–Stout disease (GSD) is a rare disorder of unknown etiology. We present a 6-year-old male with GSD involving the skull base who presented with recurrent cerebrospinal fluid (CSF) rhinorrhea, severe hearing loss, and facial palsy secondary to cerebellar herniation into the internal auditory canal. After 2 months of treatment with pegylated interferon (IFN) α-2b (50 μg/week), his hearing recovered dramatically. Two years later, new bone formation appeared radiologically and IFN was switched to sirolimus. One year after the switch, CSF rhinorrhea disappeared. Antiangiogenic therapy might inhibit proliferation of vascular endothelial cells in osteolytic lesions and lead to new bone formation. Pediatr Blood Cancer © 2015 Wiley Periodicals, Inc.

Key words: cerebrospinal fluid leakage; interferon; lymphatic malformation; mammalian target of rapamycin; sirolimus

INTRODUCTION

Gorham–Stout disease (GSD), also known as massive osteolysis, is a rare bone disorder of unknown etiology originally described in the 1950s.[1] Aggressive lymphatic and vascular proliferation of unknown origin is believed to be the cause of local bone destruction. Michael et al. summarized the clinical information from 185 previously published cases of GSD and found skull base involvement in only nine cases.[2] GSD has a risk of fatal complications. Spinal cord damage and paraplegia resulting from vertebral osteolysis has been reported, as has cerebrospinal fluid (CSF) leakage resulting from osteolysis of the skull.[3,4]

Optimal treatment for GSD has not yet been established. Current therapeutic modalities include surgery, interferon (IFN), and radiotherapy.[2] However, these therapies have many side effects, and treatment strategy remains controversial. Since 2009, a FDA-funded prospective trial of sirolimus, a mammalian target of rapamycin (mTOR) inhibitor, has been underway for treatment of complicated vascular anomalies (ClinicalTrials.gov NCT00975819).[5] mTOR is a serine/threonine kinase regulated by phosphoinositide 3-kinase. It acts as a master switch for numerous cellular processes, including cellular catabolism and anabolism, cell motility, angiogenesis, and cell growth.[6] Recently, the successful use of mTOR inhibitors in treating a small number of lymphatic anomalies has been reported.[7] Therefore, we hypothesized that sirolimus might be a promising treatment for GSD.

Here, we present the case of a child with GSD involving the skull base who presented with CSF leakage, severe hearing loss, and facial palsy secondary to herniation of cerebellar tissue into the internal auditory canal (IAC). Systemic medication could improve symptoms and result in new bone formation. We also discuss this rare condition and the mechanism of recovery.

CASE REPORT

A 3-year-old male presented with a history of repeated CSF rhinorrhea and bacterial meningitis, with left ear deafness as a complication of bacterial meningitis. He was diagnosed with basal meningoencephalocele; surgical repair of the CSF fistula at the anterior skull base was performed at another hospital when the patient was 4 years old. However, he experienced refractory CSF rhinorrhea and bacterial meningitis. When the patient was 6 years old, a skull base biopsy showed resorption of typical bone structures, which had been replaced by thin-walled endothelium-lined capillaries of vascular or lymphatic origin (Fig. 1A). D2-40 immunostaining delineated the endothelium of the lymphatic channels and a diagnosis of GSD was made (Fig. 1B). Six months after biopsy, the patient presented with acute right-sided hearing loss and mild peripheral facial palsy. Because these symptoms persisted for 3 months, he was transferred to our hospital for additional therapy.

The patient had mild right facial nerve palsy (House–Brackmann Facial Nerve Grading System, Grade II, mild dysfunction) and repeated CSF rhinorrhea several times daily. Puretone audiogram demonstrated severe sensorineural hearing loss

Abbreviations: GSD, Gorham–Stout disease; CSF, cerebrospinal fluid; IFN, interferon; FDA, Food and Drug Administration; mTOR, mammalian target of rapamycin; IAC, internal auditory canal; CT, computed tomography; MRI, magnetic resonance imaging; VEGF, vascular endothelial growth factor

[1]Department of Pediatrics, Graduate School of Medicine, Gifu University, Gifu, Japan; [2]Department of Otolaryngology, Graduate School of Medicine, Gifu University, Gifu, Japan; [3]Department of Radiology, Graduate School of Medicine, Gifu University, Gifu, Japan; [4]Department of Pathology, National Center for Child Health and Development, Tokyo, Japan

Grant sponsor: Grant-in-Aid for Scientific Research from the Ministry of Education, Culture, Sports, Science and Technology of Japan; Grant number: 25461587; Grant sponsor: Health and Labour Science Research Grant for Research on Intractable Diseases from the Ministry of Health, Labour and Welfare of Japan (to M.O.); Grant sponsor: Practical Research Project for Rare/Intractable Diseases from Japan's Agency for Medical Research and Development, AMED (15Aek0109057h0102).

Conflict of interest: Nothing to declare.

*Correspondence to: Michio Ozeki, Department of Pediatrics, Graduate School of Medicine, Gifu University, Yanagido 1-1, Gifu 501-1194, Japan; E-mail: michioo@gifu-u.ac.jp

Received 13 October 2015; Accepted 4 December 2015

DOI 10.1002/pbc.25886
Published online in Wiley Online Library (wileyonlinelibrary.com).

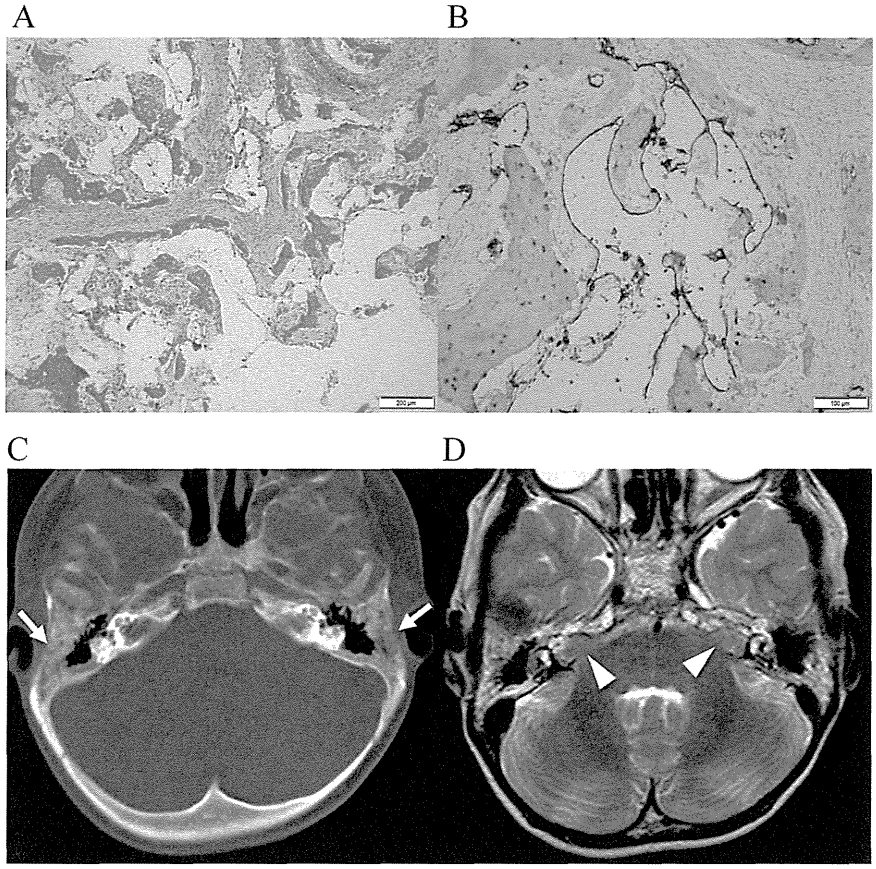

Fig. 1. Pathological examination of the affected lesion and radiological examination of the patient before treatment. (**A**) Skull base biopsy showing that typical bone structures were resorbed and replaced by thin-walled endothelium-lined capillaries of vascular or lymphatic origin (bar 200 μm, hematoxylin and eosin). (**B**) Immunopathological examination positive for lymphatic marker D2-40 (bar 100 μm). (**C**) Axial noncontrast CT of temporal bones revealed diffuse osteolysis (arrow) and severe expansion of the IAC. (**D**) Axial noncontrast T2-weighted MRI revealed herniation of the cerebellar tissue into the IAC (arrowhead).

of the right ear. Auditory-evoked brain response testing of the right ear showed no waveforms at 130 dB sound pressure level. Computed tomography (CT) of the head showed multiple lytic lesions in the temporal bones and expansion of the bilateral IACs (Fig. 1C). Magnetic resonance imaging (MRI) of the skull base demonstrated herniation of cerebellar tissue into the bilateral IACs (Fig. 1D). Radioisotope cisternography with In-111 showed CSF leakage. Because the patient's condition was severe and progressive, we decided to treat with pegylated IFN α-2b. The treatment was approved by the review board at our hospital and written informed consent was obtained from the patient's parents. We started pegylated IFN α-2b (50 μg, 1.5 μg/kg) once weekly, according to a reported protocol.[8] Two months later, the patient's hearing in the right ear recovered dramatically. His audiogram also showed marked improvement. Auditory-evoked brain response showed restoration of I–V waves. Facial nerve function improved to Grade I. However, MRI and CT showed no marked changes in the temporal bones. Six months after initiation of IFN therapy, CT revealed slight new bone formation in the bilateral temporal bones. Two years after IFN therapy was initiated, bone formation was clearly identified in the bilateral temporal bones (Fig. 2A). MRI showed improvement of cerebellar herniation (Fig. 2B). Because the patient had side effects with IFN treatment (high fever, fatigue, and mild depression), the patient and his family wanted to taper the medication. Additionally, the patient continued to experience recurrent CSF rhinorrhea. A clinical study of sirolimus for the treatment of complex vascular anomalies has been underway at our hospital since 2014. We decided to switch this patient's therapy from IFN to sirolimus to minimize side effects and to treat his recurrent CSF rhinorrhea. Written informed consent for this treatment was obtained from the patient's parents.

Sirolimus was added at 1.6 mg/m^2 once daily. Dose adjustments were made to maintain the desired 24-h trough level at 10–15 ng/ml. After 6 months of sirolimus treatment, the frequency of CSF rhinorrhea decreased to once monthly and IFN therapy was discontinued. One year later, the patient's CSF rhinorrhea disappeared completely. Radioisotope cisternography with In-111 showed little leakage of CSF. At 3-year follow-up, the patient had been taking sirolimus for over 1 year without any adverse effects and had good facial nerve function and hearing.

DISCUSSION

Our patient with GSD not only had CSF rhinorrhea, but also sudden severe hearing loss and facial palsy caused by herniation

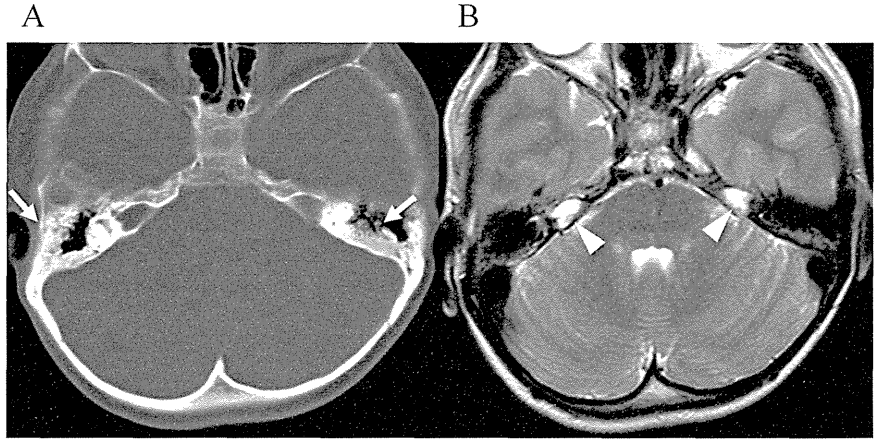

Fig. 2. Radiological examination of the patient 2 years after initiation of interferon therapy and prior to sirolimus treatment. (**A**) Axial noncontrast CT revealed an obvious increase in bone density of the mastoid air cells (arrow). (**B**) Axial noncontrast T2-weighted MRI revealed improvement of cerebellar hernia (arrowhead).

of cerebellar tissue into the right IAC, as a result of an osteolytic lesion of the skull base causing bone fragility. His hearing disturbance and CSF rhinorrhea resolved completely, and new bone was formed in the osteolytic lesion.

The pathogenesis of GSD is poorly understood. There are only three reported cases of hearing loss secondary to GSD.[9–11] In one of these patients, hearing loss was caused by an osteolytic lesion directly infiltrating the cochlear duct. However, the causes of hearing loss in the other two patients were unclear. Hearing was not restored in these patients. We believe that our rare experience provides important insights into the pathogenesis of GSD.

In our patient, cochlear nerve dysfunction and facial nerve palsy developed and resolved concurrently. Patients with cerebellopontine angle meningioma with IAC involvement present with hearing loss and abnormal facial motor function, clinical manifestations caused by compression neuropathy rather than parenchymal involvement.[12,13] It is hypothesized that compression neuropathy results in biochemical changes within the axons and Schwann sheaths of the cerebral nerve, and that segmental demyelination may be implicated.[14] Our patient also had herniation of cerebellar tissue into the IAC, and there was marked reduction of cerebellar herniation when hearing loss recovered. We believe that cerebellar herniation might have caused compression neuropathy of the cochlear and facial nerves. Improvement in cerebellar herniation thus could result in concurrent resolution of hearing loss and facial palsy.

Antiosteoclastic medications (bisphosphonates) are often used to treat GSD.[2] We did not administer bisphosphonates in the present case because the biopsy specimen did not show the presence of osteoclasts or activation of these cells. Instead, our patient received antiangiogenic therapy with pegylated IFN α-2b and sirolimus. Recent studies have suggested that vascular proliferation might be related to the pathogenesis of bone resolution in GSD patients.[15,16] IFN might downregulate expression of vascular endothelial growth factor (VEGF).[17] The mTOR inhibitor sirolimus targets protein synthesis downstream of the Akt pathway and is predicted to be effective in disorders where the mTOR growth control pathway is affected.[6] mTOR is overexpressed in some vascular malformations; mTOR inhibitors exert their antiangiogenic activity in tumors by impairing production of VEGF.[18] This patient experienced new bone formation and disappearance of CSF rhinorrhea after drug treatment. Radiological examination revealed an obvious increase in bone density (Fig. 2A). The precise mechanism of new bone formation is unknown. We speculate that antiangiogenic therapy inhibited proliferation of vascular and lymphatic endothelial cells in the osteolytic lesion and led to new bone formation and disappearance of CSF rhinorrhea.

In conclusion, we present the case of a child with GSD involving the skull base who presented with CSF leakage, severe hearing loss, and facial palsy secondary to herniation of cerebellar tissue into the IAC. Antiangiogenic therapy might inhibit proliferation of vascular endothelial cells in osteolytic lesions and lead to new bone formation.

ACKNOWLEDGMENTS

We thank Dr. Nobuyuki Yotani and Dr. Nobuhito Morota at the National Center for Child Health and Development and Dr. Toshiya Kamiya at Matsuzaka General Hospital for their helpful comments. We also thank the Department of Pediatrics at Gifu University for their contribution. The present study was supported in part by a Grant-in-Aid for Scientific Research from the Ministry of Education, Culture, Sports, Science and Technology of Japan (25461587); a Health and Labour Science Research Grant for Research on Intractable Diseases from the Ministry of Health, Labour and Welfare of Japan received by M.O.; and Practical Research Project for Rare/Intractable Diseases from Japan's Agency for Medical Research and Development, AMED (15Aek0109057h0102).

REFERENCES

1. Gorham LW, Wright AW, Shultz HH, Maxon FC Jr. Disappearing bones: A rare form of massive osteolysis: Report of two cases, one with autopsy findings. Am J Med 1954;17:674–682.
2. Dellinger MT, Garg N, Olsen BR. Viewpoints on vessels and vanishing bones in Gorham–Stout disease. Bone 2014;13:47–52.
3. Halliday DR, Dahlin DC, Pugh DG, Young HH. Massive osteolysis and angiomatosis. Radiology 1964;82:637–644.
4. Iyer GV. Cerebrospinal fluid rhinorrhoea from massive osteolysis of the skull. J Neurol Neurosurg Psychiatry 1979;42:767–769.

5. Hammill AM, Wentzel M, Gupta A, Nelson S, Lucky A, Elluru R, Dasgupta R, Azizkhan RG, Adams DM. Sirolimus for the treatment of complicated vascular anomalies in children. Pediatr Blood Cancer 2011;57:1018–1024.
6. Vignot S, Faivre S, Aguirre D, Raymond E. mTOR-targeted therapy of cancer with rapamycin derivatives. Ann Oncol 2005;16:525–537.
7. Lackner H, Karastaneva A, Schwinger W, Benesch M, Sovinz P, Seidel M, Sperl D, Lanz S, Haxhija E, Reiterer F, Sorantin E, Urban CE. Sirolimus for the treatment of children with various complicated vascular anomalies. Eur J Pediatr 2015; 174:1579–1584.
8. Ozeki M, Funato M, Kanda K, Ito M, Teramoto T, Kaneko H, Fukao T, Kondo N. Clinical improvement of diffuse lymphangiomatosis with pegylated interferon alfa-2b therapy: Case report and review of the literature. Pediatr Hematol Oncol 2007;24: 513–524.
9. Girn HR, Towns G, Chumas P, Holland P, Chakrabarty A. Gorham's disease of skull base and cervical spine–confusing picture in a two year old. Acta Neurochir 2006;148:909–913.
10. Cushing SL, Ishak G, Perkins JA, Rubinstein JT. Gorham–Stout syndrome of the petrous apex causing chronic cerebrospinal fluid leak. Otol Neurotol 2010;31:789–792.
11. Morimoto N, Ogiwara H, Miyazaki O, Kitamuara M, Nishina S, Nakazawa A, Maekawa T, Morota N. Gorham–Stout syndrome affecting the temporal bone with cerebrospinal fluid leakage. Int J Pediatr Otorhinolaryngol 2013;77:1596–1600.
12. Gao K, Ma H, Cui Y, Chen X, Ma J, Dai J. Meningiomas of the cerebellopontine angle: Radiological differences in tumors with internal auditory canal involvement and their influence on surgical outcome. PLoS ONE 2015;10:e0122949.
13. Hu YF, Cheng PW, Young YH. Comparison of vestibular function between large cerebellopontine angle meningioma and schwannoma. Acta Otolaryngol 2009;129:161–165.
14. Neely JG. Reversible compression neuropathy of the eighth cranial nerve from a large jugular foramen schwannoma. Arch Otolaryngol 1979;105:555–560.
15. Radhakrishnan K, Rockson SG. Gorham's disease: An osseous disease of lymphangiogenesis? Ann N Y Acad Sci 2008;1131:203–205.
16. Hagendoorn J, Padera TP, Yock TI, Nielsen GP, di Tomaso E, Duda DG, Delaney TF, Gaissert HA, Pearce J, Rosenberg AE, Jain RK, Ebb DH. Platelet-derived growth factor receptor-beta in Gorham's disease. Nat Clin Pract Oncol 2006;3:693–697.
17. Cano B, Insa S, Cifrián C, Cortina H, Hernández M. Radiologic findings in Gorham–Stout syndrome. Radiologia 2006;48:33–36.
18. Shirazi F, Cohen C, Fried L, Arbiser JL. Mammalian target of rapamycin (mTOR) is activated in cutaneous vascular malformations *in vivo*. Lymphat Res Biol 2007;5:233–236.

Article

Developmental Cell

APJ Regulates Parallel Alignment of Arteries and Veins in the Skin

Graphical Abstract

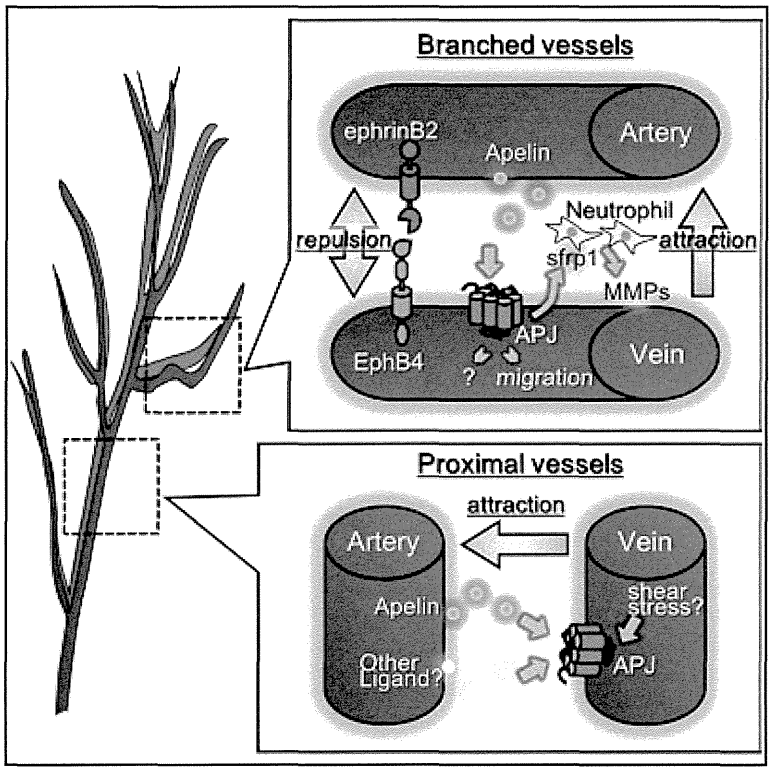

Authors

Hiroyasu Kidoya, Hisamichi Naito, ..., Akiyoshi Fukamizu, Nobuyuki Takakura

Correspondence

ntakaku@biken.osaka-u.ac.jp

In Brief

Molecular mechanisms for control of parallel arterial-venous (A-V) alignment and the function of A-V juxtaposition have not been elucidated. Kidoya et al. show that apelin produced from arterial endothelial cells (ECs) stimulates APJ expressed on venous ECs to induce A-V alignment and that this alignment is involved in thermoregulation.

Highlights

- *Apelin* or *APJ* mutant mice have abnormal arterial-venous (A-V) alignment
- Apelin from arterial endothelial cells (ECs) induces chemotaxis of APJ^{+} venous ECs
- Venous ECs induce neutrophil production of MMP-9, allowing for EC migration
- Mice with defective A-V alignment have defects in thermoregulation

Kidoya et al., 2015, Developmental Cell *33*, 247–259
May 4, 2015 ©2015 Elsevier Inc.
http://dx.doi.org/10.1016/j.devcel.2015.02.024

Developmental Cell
Article

APJ Regulates Parallel Alignment of Arteries and Veins in the Skin

Hiroyasu Kidoya,[1] Hisamichi Naito,[1] Fumitaka Muramatsu,[1] Daishi Yamakawa,[1] Weizhen Jia,[1] Masahito Ikawa,[2] Takashi Sonobe,[3] Hirotsugu Tsuchimochi,[3] Mikiyasu Shirai,[3] Ralf H. Adams,[4,5] Akiyoshi Fukamizu,[6] and Nobuyuki Takakura[1,7,*]

[1]Department of Signal Transduction
[2]Animal Resource Center for Infectious Diseases
Research Institute for Microbial Diseases, Osaka University, 3-1 Yamada-oka, Suita, Osaka 565-0871, Japan
[3]Department of Cardiac Physiology, National Cerebral and Cardiovascular Center Research Institute, 5-7-1 Fujishirodai, Suita, Osaka 565-8565, Japan
[4]Department of Tissue Morphogenesis, Max Planck Institute for Molecular Biomedicine, 48149 Muenster, Germany
[5]Faculty of Medicine, University of Muenster, 48149 Muenster, Germany
[6]Life Science Center, Tsukuba Advanced Research Alliance, The University of Tsukuba, 1-1-1 Tennoudai, Tsukuba, Ibaraki 305-8577, Japan
[7]Core Research for Evolutional Science and Technology, Japan Science and Technology Agency, K's Gobancho, 7 Gobancho, Chiyoda-ku, Tokyo 102-0076, Japan
*Correspondence: ntakaku@biken.osaka-u.ac.jp
http://dx.doi.org/10.1016/j.devcel.2015.02.024

SUMMARY

Molecular pathways regulating the development of arterial and venous endothelial cells (ECs) are now well established, but control of parallel arterial-venous alignment is unclear. Here we report that arterial-venous alignment in the skin is determined by apelin receptor (APJ) expression in venous ECs. One of the activators of APJ is apelin. We found that apelin is produced by arterial ECs during embryogenesis, induces chemotaxis of venous ECs, and promotes the production of secreted Frizzled-related protein 1 (sFRP1) by APJ$^+$ ECs. sFRP1 stimulates matrix metalloproteinase production by Ly6B.2$^+$ neutrophil-like cells located between the arteries and veins, resulting in remodeling of extracellular matrices to support venous displacement. Moreover, using *apelin*- or *APJ*-deficient mice, which exhibit arterial-venous disorganization, we found that arterial-venous alignment is involved in thermoregulation, possibly by regulating countercurrent heat exchange. We hypothesize that the evolution of parallel juxtapositional arterial-venous alignment was an adaptation to reduce body heat loss.

INTRODUCTION

The formation of a complex and diverse vascular system is critical for maintaining homeostasis in vertebrates because of its function in transportation of nutrients and oxygen throughout the body. In adult peripheral tissues, alignment of arteries, veins, and nerves is visible anatomically and is considered to have some physiological function. Morphological and genetic evidence suggests that the signals from cells composing blood vessels and the nervous system may together determine the appropriate patterning and branching of the vascular network (Carmeliet, 2003). Local signals produced from peripheral nerves control arterial differentiation and provide a template that determines the organotypic patterning of arteriogenesis in the skin of the embryonic mouse limb (Mukouyama et al., 2002) and prechondrogenic mesenchyme (Bates et al., 2003). Genetic studies showed that vascular endothelial growth factor (VEGF) derived from sensory neurons, motoneurons, and/or Schwann cells plays central roles in arteriogenesis from a primitive capillary plexus in vivo (Mukouyama et al., 2005). Although these studies have documented intimate associations and functional interactions between nerve and artery in vascular remodeling, the mechanisms that determine the alignment of veins and arteries have not been elucidated.

Arteries and veins were previously identified by their morphological appearance and function, and more recently also by molecular differences (Lin et al., 2007). Arterial-specific ephrinB2 is a ligand for the venous-specific EphB4 receptor; this system regulates the establishment and maintenance of arterial-venous (A-V) plexus and distinct boundaries between these vessels by repulsive effects (Klein, 2004; Pasquale, 2005; Poliakov et al., 2004). Repulsion is a major mechanism for maintaining distance between arteries and veins; however, the molecular mechanisms responsible for such juxtapositioning have not yet been determined.

Countercurrent heat exchange between closely juxtaposed arteries and veins would have a significant effect on regulation and maintenance of core temperature (Bazett et al., 1948a, 1948b; Mitchell and Myers, 1968). In a cold environment, arterial blood would be cooled prior to entering the peripheral capillary beds by heat transfer to the venous blood and, vice versa, the latter would be warmed before returning to the core of the body. This would reduce heat loss, which might otherwise occur as capillary bed blood passes into extremities with large surface areas. Thus, it is hypothesized that A-V alignment is closely related to thermoregulation, but in vivo experimental evidence in support of this notion is largely lacking.

Apelin, an endogenous ligand for the apelin receptor (APJ), has a wide range of physiological roles, including regulation of

cardiovascular function, fluid homeostasis, effects on the adipoinsular axis, and angiogenesis (Boucher et al., 2005; Lee et al., 2000; Roberts et al., 2009). We previously showed that the apelin/APJ system is involved in maturation of blood vessels by regulating caliber size modification and permeability during angiogenesis (Kidoya et al., 2008, 2010; Takakura and Kidoya, 2009). In *Xenopus laevis* and zebrafish embryos, expression of an *APJ* gene ortholog is observed in the venous vasculature (Kälin et al., 2007; Tucker et al., 2007). In the neonatal mouse retina, APJ expression is upregulated in endothelial cells (ECs) of the venous vessels during angiogenesis, and this suggests that the apelin/APJ system plays a spatiotemporal role in blood vessel formation (Saint-Geniez et al., 2003).

In the present study, we analyzed the role of apelin/APJ signaling for A-V interactions and how arteries and veins align during vascular remodeling in the mouse embryo.

RESULTS

Involvement of the Apelin/APJ System in A-V Alignment for Vascular Formation

To determine the temporal and spatial expression of APJ and apelin in blood vessels of mouse embryos, we initially performed an immunohistochemical analysis of the skin of the back because whole-vessel structure can be observed in this location. At embryonic day (E)15.5, APJ expression was colocalized with EphB4, a venous endothelial-specific molecule (Figure 1A). In contrast, immunohistochemistry and in situ hybridization revealed that apelin protein and *apelin* transcripts were present in arterial blood vessels covered with α-smooth muscle actin (SMA)-positive cells (Figure 1B; Figures S1A and S1B). Larger veins often localized together with arteries in E15.5 skin, and expression of apelin and APJ was seen in adjacent arteries and veins, respectively (Figure 1D). These results suggest that the apelin/APJ system is active during angiogenesis and may contribute to A-V network formation.

Next, using *apelin*$^{-/-}$ or *APJ*$^{-/-}$ adult mice, we investigated the effects of apelin/APJ signaling deficiency on A-V formation. As with embryonic skin, veins are aligned with arteries, and the branching pattern of arteries and veins is similar in the back skin of adult wild-type mice. In *apelin*$^{-/-}$ mice, although large venules and arterioles were proximately localized, the pattern of branches from those vessels was quite different between arterioles and venules. Even more strikingly, arterioles and venules completely dissociated from one another in *APJ*$^{-/-}$ mice (Figures 1E and 1F). However, intercostal, cervical, and tail vasculature appeared to be formed normally (Figure S1C). Severe A-V misalignment in *APJ*$^{-/-}$ mice compared with *apelin*$^{-/-}$ mice was also observed by microangiography of the femoral and popliteal vessels (Figure 1G). We previously reported that apelin/APJ signaling regulates capillary but not arteriole and venule caliber size. This was accomplished using *apelin*$^{-/-}$ mice and transgenic mice in which apelin was overexpressed under the transcriptional control of the K14 promoter. However, we had not noticed the disorganized A-V alignment as seen above in *apelin*$^{-/-}$ mice in our previous reports (Kidoya et al., 2008, 2010). Moreover, in addition to capillary formation, we had not found any defects in the formation and structure of arterioles and venules in *apelin*$^{-/-}$ mice (Kidoya et al., 2008). Consistent with this, arteries and veins themselves are well developed in adult *apelin*$^{-/-}$ or *APJ*$^{-/-}$ mice (Figure 1E). We therefore propose that the apelin/APJ system, especially APJ, is required for regulation of parallel juxtapositional alignment of arterioles and venules in skin. To confirm that apelin produced by arteries truly drives venous alignment, we created mice lacking apelin only in their arteries using an artery-specific Cre driver (*Bmx(PAC)-Cre ERT2* transgenic) and floxed *apelin* mice (Ehling et al., 2013). Artery-specific apelin gene deletion from E10.5 onward led to abnormal A-V alignment similar to conventional *apelin* knockouts (Figures S1D–S1F).

Apelin Deficiency Abrogates Proper A-V Alignment

To further investigate how parallel juxtapositional alignment of arteries and veins is induced during the process of vascular remodeling, we analyzed the time course of vascular development in the skin of the backs of mouse embryos using a whole-mount immunohistochemical technique.

At E13.5, SMA$^+$ arteries and morphologically indistinguishable veins cannot yet be identified in the capillary plexus. By E14.0, αSMA$^+$ cells emerged and gradually overlaid CD31$^+$ ECs, inducing arterial commitment (Figure 2A). By E14.5, blood vessels expressing APJ had emerged but did not localize with SMA$^+$ arteries. Subsequently, from E14.5 through E15.5, APJ-strongly positive veins emerged and gradually became aligned next to arteries, and complete alignment was established at around E16.5. In contrast to wild-type mice, APJ$^+$ veins and αSMA$^+$ arteries of distal infrascapular vessels were still separated at E16.5 in *apelin*$^{-/-}$ embryos (Figures 2B and 2C). During the patterning process of these vessels, apelin was synchronously expressed in arterial blood vessels just after mural cell coverage begins at E14.0 in the embryo (Figure 2D).

Several studies have shown that apelin/APJ signaling induces angiogenesis in the retinal vasculature (Kälin et al., 2007; Kasai et al., 2004). Therefore, it is possible that insufficient blood vessel formation affects A-V alignment; however, there are no significant differences between wild-type, *apelin*$^{-/-}$, and *APJ*$^{-/-}$ mice regarding vascular density, number of branches, vessel length in the skin, and arterial and venous EC differentiation (Figures 2A and 2B; Figures S2A and S2B).

For arteriogenesis, VEGF derived from peripheral nerves is necessary for arterial differentiation and patterning of arterial branching (Mukouyama et al., 2002, 2005). However, the association between arteries and peripheral nerves in the dermis of E15.5 embryos was unaffected in the absence of apelin/APJ signaling (Figure S2C). Moreover, lymphatic vessels in the dermis of E15.5 is unaffected by the lack of apelin/APJ signaling (Figure S2D). Taken together, these observations suggest that apelin/APJ is involved in A-V alignment directly, that is, apelin, which is secreted by arterial ECs, acts on APJ-expressing neighboring venous ECs.

During the process of appropriate A-V parallel juxtapositional alignment, movement of ECs and matrix remodeling are required. To confirm the influence of APJ signaling on the mobility of venous vascular ECs, we injected Matrigel plugs containing apelin or VEGF into mice. We observed that a large number of ECs migrated into apelin-containing Matrigel. This was seen to a similar extent with VEGF but only in wild-type mice, not *APJ*$^{-/-}$ mice (Figures S2E and S2F). Expression of venous marker mRNAs (*APJ*, *EphB4*, and *COUP-TF2*) was significantly

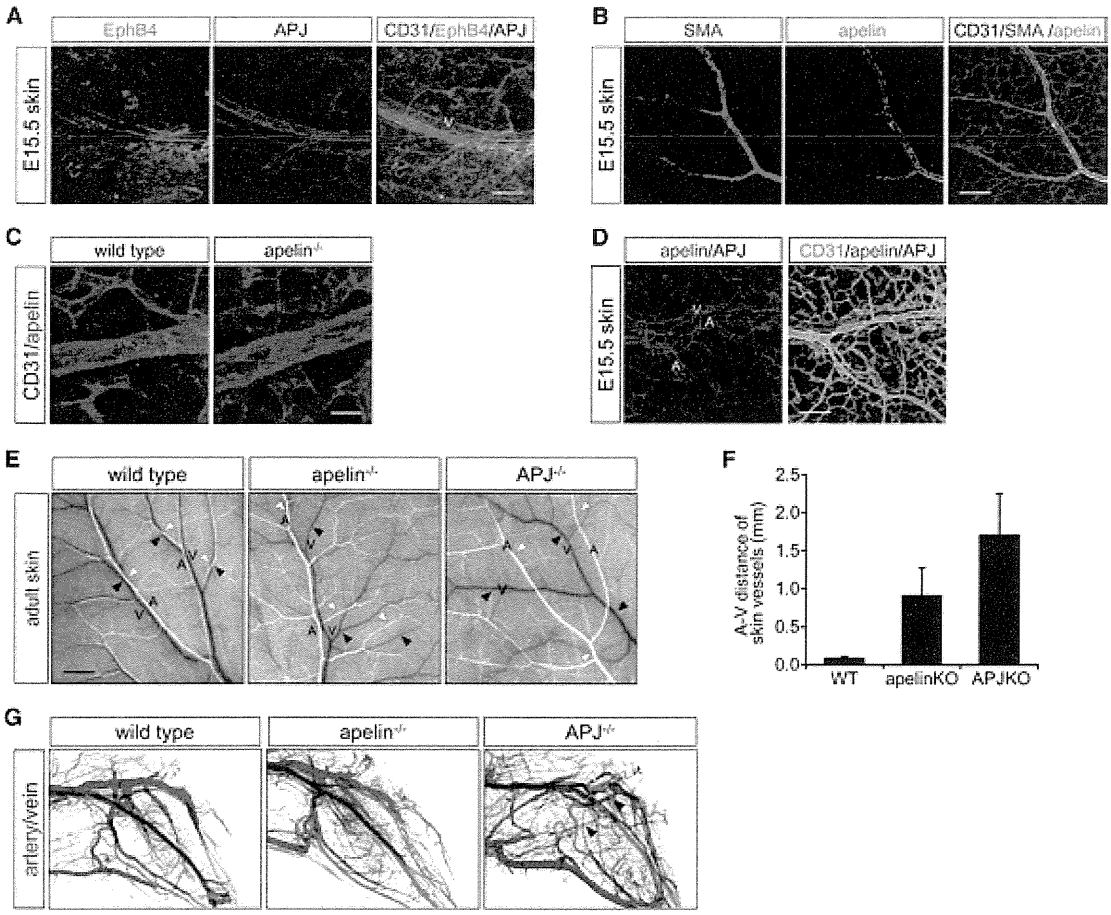

Figure 1. Apelin and APJ Expression in Arterial and Venous ECs and Phenotype of *Apelin* and *APJ* Mutant Mice

(A) CD31 (red), EphB4 (green), and APJ (blue) staining of the back skin of an E15.5 mouse embryo. The scale bar represents 100 μm. V, vein.

(B) Detection of *apelin* transcripts (green) in the back skin of an E15.5 mouse embryo by in situ hybridization with CD31 (blue) and αSMA (red). The scale bar represents 200 μm.

(C) Apelin (red) and CD31 (blue) staining of skin from the back of an E14.5 mouse embryo. The scale bar represents 100 μm.

(D) Apelin (red), APJ (blue), and CD31 (green) staining of back skin of an E14.5 mouse embryo. The scale bar represents 100 μm. A, artery.

(E) Gross appearance of blood vessels in the back skin of adult (7–8 weeks of age) wild-type, *apelin*$^{-/-}$, and *APJ*$^{-/-}$ mice. Arterial blood vessels were identified by injecting barium into the left ventricle. Black and white arrowheads indicate veins and arteries, respectively. The scale bar represents 2 mm in the back skin.

(F) Quantitative evaluation of the distance between the artery and vein of distal infrascapular vessels in the back skin of wild-type, *apelin*$^{-/-}$, and *APJ*$^{-/-}$ mice. Data represent the average ± SD; n = 12 from four mice per group. $p < 0.01$. KO, knockout.

(G) Microangiograms in the hindlimb from 8-week-old wild-type, *apelin*$^{-/-}$, and *APJ*$^{-/-}$ mice. Arterial blood vessels were identified by injecting barium into the left ventricle. White and black arrowheads in *APJ*$^{-/-}$ mice indicate peripheral arteries and veins, respectively.

See also Figure S1.

higher in ECs infiltrating into apelin-containing plugs compared with those from VEGF-containing plugs (Figure 2E; Figures S2E–S2G). Furthermore, we performed in vitro Transwell migration assays using apelin or VEGF as chemoattractants for ECs collected from the back skin of embryos. Consistent with previously published data (Kasai et al., 2004), migration of wild-type ECs in response to apelin or VEGF stimulation was observed (Figure S2H). Those wild-type ECs migrating toward apelin expressed higher levels of *APJ* and *EphB4* mRNA but lower *ephrinB2* compared with those attracted by VEGF (Figure S2I). Taking the data together, we conclude that apelin/APJ signaling is a crucial regulator of migration of venous ECs and contributes to the translocation of veins.

Involvement of Extracellular Matrix Degradation in Venous Vascular Displacement

Modification of tissue morphogenesis, especially remodeling of three-dimensional extracellular matrices (ECMs) by proteolytic degradation, is necessary for the remodeling of blood vessels including juxtapositional regulation between artery and vein (Friedl and Gilmour, 2009). Therefore, we tested the effect of ECM degradation on the remodeling of venous vascular displacement modulated by apelin/APJ signaling. In skin from E14.0 embryos, individual blood vessels were covered with type IV collagen to a similar extent (Figure 3A). However, in skin from E14.5 embryos, the amount of type IV collagen around APJ^{+} veins that were being attracted toward arteries was

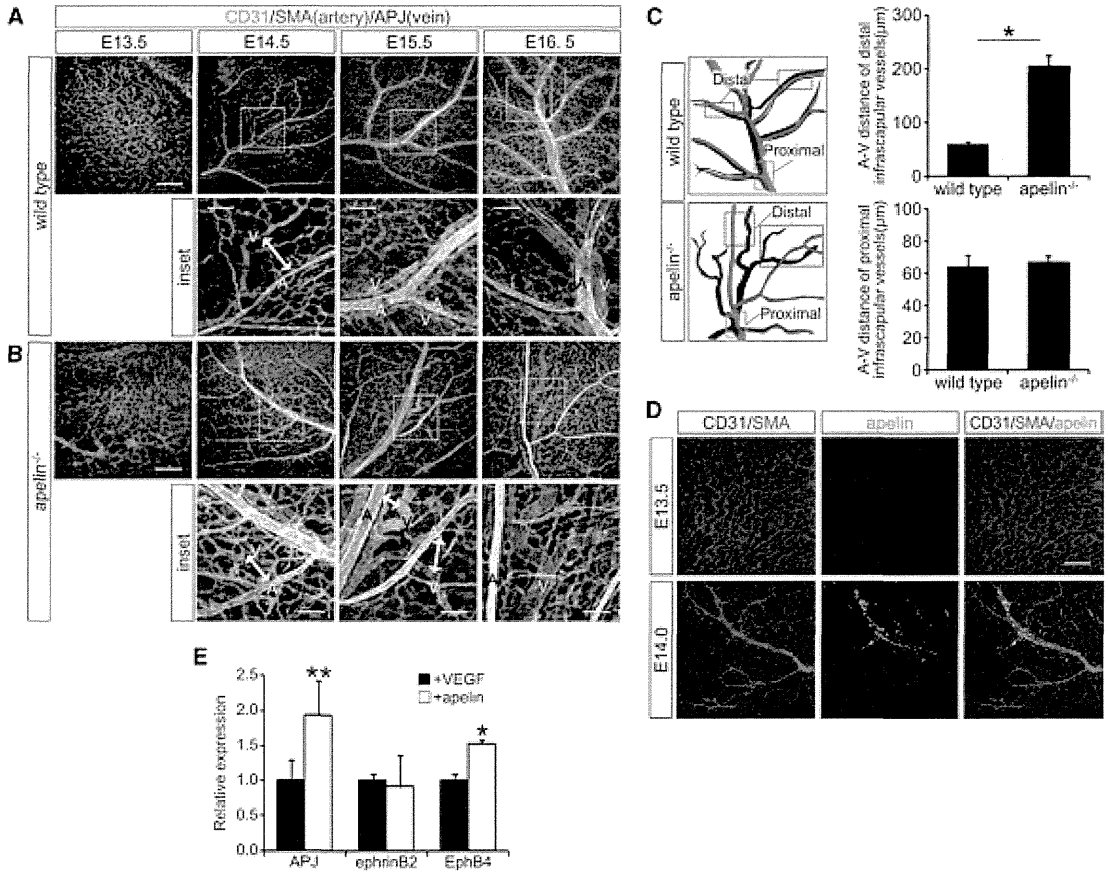

Figure 2. Arterial-Venous Remodeling in Skin during Embryogenesis

(A and B) CD31 (green), αSMA (red), and APJ (blue) expression in the back skin from mouse embryos at several developmental stages as indicated. Wild-type (A) and *apelin*$^{-/-}$ (B) mice. Images below show a higher magnification of the areas indicated by the boxes. Note that veins are located separately from arteries at E14.5 (white arrows) and gradually move close to arteries at E14.5 and E15.5 stages in wild-type but generally not in *apelin*$^{-/-}$ mice. The scale bars represent 300 μm and 100 μm (insets).

(C) Quantitative evaluation of the distance between the artery and vein of distal and proximal infrascapular vessels in skin from the backs of E16.5 wild-type or *apelin*$^{-/-}$ embryos. Data are means ± SD; n = 18 (distal) or 12 (proximal) from six mice per group. *$p < 0.01$.

(D) Immunohistochemical analysis of apelin expression in the back skin of E13.5 and E14.0 mouse embryos. Blood vessels were stained with anti-CD31 (blue) and smooth muscle cells with anti-αSMA (red) Abs. Note that apelin (green) was specifically expressed in arteries covered by smooth muscle cells.

(E) Relative expression of arterial (*ephrinB2*)- or venous (*EphB4*)-specific marker mRNA in ECs recruited into the Matrigel plug explant by apelin or VEGF. Target gene expression levels were normalized to control gene *GAPDH*. Data represent the average ± SD; n = 3 independent experiments per group. *$p < 0.01$, **$p < 0.05$. See also Figure S2.

significantly lower in wild-type than in *apelin*$^{-/-}$ mice (Figures 3A and 3B). Because matrix metalloproteinases 2 and 9 (MMP-2 and -9) have been suggested to degrade the basement membrane during angiogenesis (van Hinsbergh et al., 2006), we sought cells producing these enzymes in embryonic skin. We found that MMP-9- and MMP-2-producing cells preferentially accumulate in the space between the arteries and veins in wild-type mice but that fewer do so in *apelin*$^{-/-}$ mice (Figure 3C). These data indicate that apelin/APJ signaling participates in controlling the expression of MMPs. Zymographic analysis revealed that MMP-2 and MMP-9 secretion into culture media was markedly stimulated when whole cells from E14.5 embryonic skin were cultured together with recombinant apelin (Figures S3A–S3F). Moreover, the expression of *MMP-2* and *MMP-9* mRNA was decreased in skin cells from *apelin*$^{-/-}$ and *APJ*$^{-/-}$ embryos relative to wild-type (Figure 3D). These results suggest that enzymatic degradation of basement membrane type IV collagen mediated by MMPs is important in apelin/APJ signaling-induced venous vascular displacement.

Although APJ is expressed only by venous ECs, which may themselves produce MMPs for degradation of matrices, EC production of MMPs was largely unaffected in *APJ*$^{-/-}$ mice except for slightly decreased expression of *MMP-2* (Figures S3G and S3H), suggesting that local MMP expression is affected in accessory cells around ECs by the deficiency of apelin or APJ. To identify the cell population producing MMP-9 and MMP-2, as observed in Figure 3C, we performed immunohistochemical analysis of back skin from E14.5 embryos. Because MMP-9 and MMP-2 are mainly secreted by mature myeloid cells, such as macrophages or neutrophils (Chung et al., 2010), we stained

for cells expressing macrophage-specific antigen F4/80 and neutrophil antigen Ly6B.2 (Rosas et al., 2010). Macrophages were found to be widely distributed in skin tissue, some of which produced MMP-2. In contrast, Ly6B.2$^+$ cells were confined to the perivenous zone and almost exclusively express MMP-9, although a small number also express MMP-2 (Figure 3E). We defined Ly6B.2$^+$ myeloid cells as neutrophil lineage cells (NLCs) because they resembled neutrophils morphologically and expressed CD11b, Gr1, and Ly6C but not Ly6G and moderately expressed F4/80 (Figures S3I and S3J). It has been suggested that this type of myeloid cell is derived from the aorta-gonad-mesonephros region and fetal liver (Schulz et al., 2012). There was no significant difference in the number of Ly6B.2$^+$ cells in the back skin of wild-type versus *apelin*$^{-/-}$ or *APJ*$^{-/-}$ littermates (Figures 3F and 3G; Figures S3M and S3N). NLCs were observed in E14.5 skin and seen to be localized between artery and vein (Figures S3K and S3L). This suggests that recruitment of Ly6B.2$^+$ cells is itself regulated by other molecules such as the chemokines produced from artery or vein tissues. Consistent with these results, the amount of *MMP-9* and *MMP-2* mRNA expression in Ly6B.2$^+$ NLCs was greatly reduced in *apelin*$^{-/-}$ or *APJ*$^{-/-}$ mice (Figures S3O and S3P). To confirm the importance of apelin/APJ signaling in ECs for the indirect induction of MMP-9 production by Ly6B.2$^+$ NLCs, we investigated whether conditioned media from ECs stimulated with apelin induced MMP-9 expression in primary Ly6B.2$^+$ NLCs in an in vitro culture model. As expected, *MMP-9* expression was upregulated by conditioned medium from apelin-stimulated wild-type but not *APJ*$^{-/-}$ ECs (Figure 3H). These results document that apelin/APJ signaling is not necessary for recruitment of Ly6B.2$^+$ NLCs to areas around the veins but is required for induction of their expression of MMPs.

Ly6B.2$^+$ NLCs and MMPs Are Essential for A-V Alignment

Several lines of evidence suggest that neutrophils actively induce tumor vascularization by secreting proangiogenic factors (Nozawa et al., 2006; Tazzyman et al., 2009). However, a role for Ly6B.2$^+$ NLCs observed in our experiments in blood vessel formation during development has not been reported previously. To this end, we depleted NLCs in pregnant mice by administering RB6-8C5, a monoclonal antibody specific for granulocyte receptor 1. We confirmed that the accumulation of Ly6B.2$^+$ NLCs in E14.5 embryo skin was markedly decreased by treatment with this antibody (Figures 4A and 4B). We then determined the effect of NLC depletion on A-V alignment. RB6-8C5 treatment resulted in partial disordering of A-V alignment, especially between the arteriolae and venulae branching from larger vessels in the skin vasculature of the adult (Figure 4C). Such abnormalities of A-V alignment were already observed in E14.5 embryo skin (Figures 4D and 4E). A-V alignments of back skin vessels were disorganized by the administration of Ilomastat, an MMP inhibitor, to pregnant mice (Figures 4F and 4G). In contrast, we could not detect any abnormality of A-V alignment in the back skin of adult *MMP-9*$^{-/-}$ mice (data not shown). These results suggest that the regulation of apelin/APJ signaling for parallel juxtapositional A-V alignment is mediated via an effect on the several MMPs produced from Ly6B.2$^+$ NLCs accumulating in the space between arteries and veins.

The Apelin-sFRP1 Axis Modulates MMP Expression

We hypothesized that stimulation of venous ECs by apelin might lead to production of factors that modulate MMP production by Ly6B.2$^+$ NLCs. To identify the key signals and factors induced by apelin/APJ signaling, we performed comprehensive mRNA expression analyses using triplicate microarrays in ECs collected from the back skin of E14.5 wild-type or *APJ*$^{-/-}$ embryos (accession number GEO: GSE66073). We applied a Student's t test filter to select gene set probes that exhibited 2-fold expression differences under a given significance level ($p < 0.05$). Subsequently, selected probes were sorted by the ratio of their expression levels in wild-type versus *APJ*$^{-/-}$ ECs, as illustrated by the heat map shown in Figure 5A. Next, we validated the expression of the selected genes by quantitative (q)RT-PCR and identified five genes significantly downregulated (*bmpr1b*, *kank1*, *madcam1*, *moxd1*, *sfrp1*) and three upregulated (*ctse*, *ptprv*, *serpina3f*) in APJ-deficient relative to wild-type mice (Figure 5B). Of these, we focused on *sfrp1*, because this gene encodes a secreted protein that has been reported to affect angiogenesis (Dufourcq et al., 2002). Secreted Frizzled-related proteins (sFRPs) are structurally similar to the Wnt receptors Frizzled proteins but lack a transmembrane region and the cytoplasmic domain. Owing to this structural property, sFRPs were first described as antagonists of the Wnt pathway that bind directly to Wnt. However, recent studies indicate that sFRPs may have additional biological functions unrelated to Wnt (Nathan and Tzahor, 2009). To assess any association of the apelin/APJ pathway with sFRP1 expression, we stimulated primary ECs from E14.5 skin with recombinant apelin in vitro. Significant induction of *sfrp1* mRNA was observed in ECs from wild-type mice within 20 hr of apelin administration (Figure 5C). This induction of *sfrp1* expression by apelin stimulation was observed in CXCR4$^-$ venous and/or microvascular ECs but not in CXCR4$^+$ arterial ECs (Figures S4A–S4C) (Li et al., 2013). Moreover, sFRP1 protein and mRNA were detected specifically in APJ$^+$ venous ECs of E14.5 skin by immunohistochemical and in situ hybridization analysis (Figure 5D; Figure S4D). To explore the biological consequences of *sfrp1* deficiency on vascular remodeling in vivo, we examined blood vessels in the skin of the backs of *sfrp1*$^{-/-}$ mice. Similar to *apelin*$^{-/-}$ and *APJ*$^{-/-}$ mice, blood vessels were normally formed but A-V parallel juxtapositional alignment was disordered in the absence of sFRP1 (Figure 5E; Figures S4E and S4F). Next, we determined whether sFRP1 induces MMP production in Ly6B.2$^+$ NLCs and macrophages collected from the skin of E14.5 embryos. We found that recombinant sFRP1 induced significant expression of *MMP-9* and *MMP-2* in Ly6B.2$^+$ NLCs and MMP-2 in macrophages (Figures 5F and 5G; Figures S4G and S4H). Consistent with these data, the number of MMP-9- and MMP-2-producing Ly6B.2$^+$ NLCs was decreased in E14.5 *sfrp1*$^{-/-}$ embryos (Figures S3M–S3P). A role for sFRP1 in the induction of MMP-9 production via the apelin pathway was confirmed by evidence that *MMP-9* expression in Ly6B.2$^+$ NLCs was not induced by medium conditioned by *sfrp1*$^{-/-}$ ECs stimulated with apelin (Figure 5H). Taken together, these results indicate that sFRP1 is upregulated in venous ECs via APJ activation by apelin released from arterial ECs and induces MMP production in adjacent Ly6B.2$^+$ NLCs. Because these reside beside venous ECs, this results in ECM degradation to

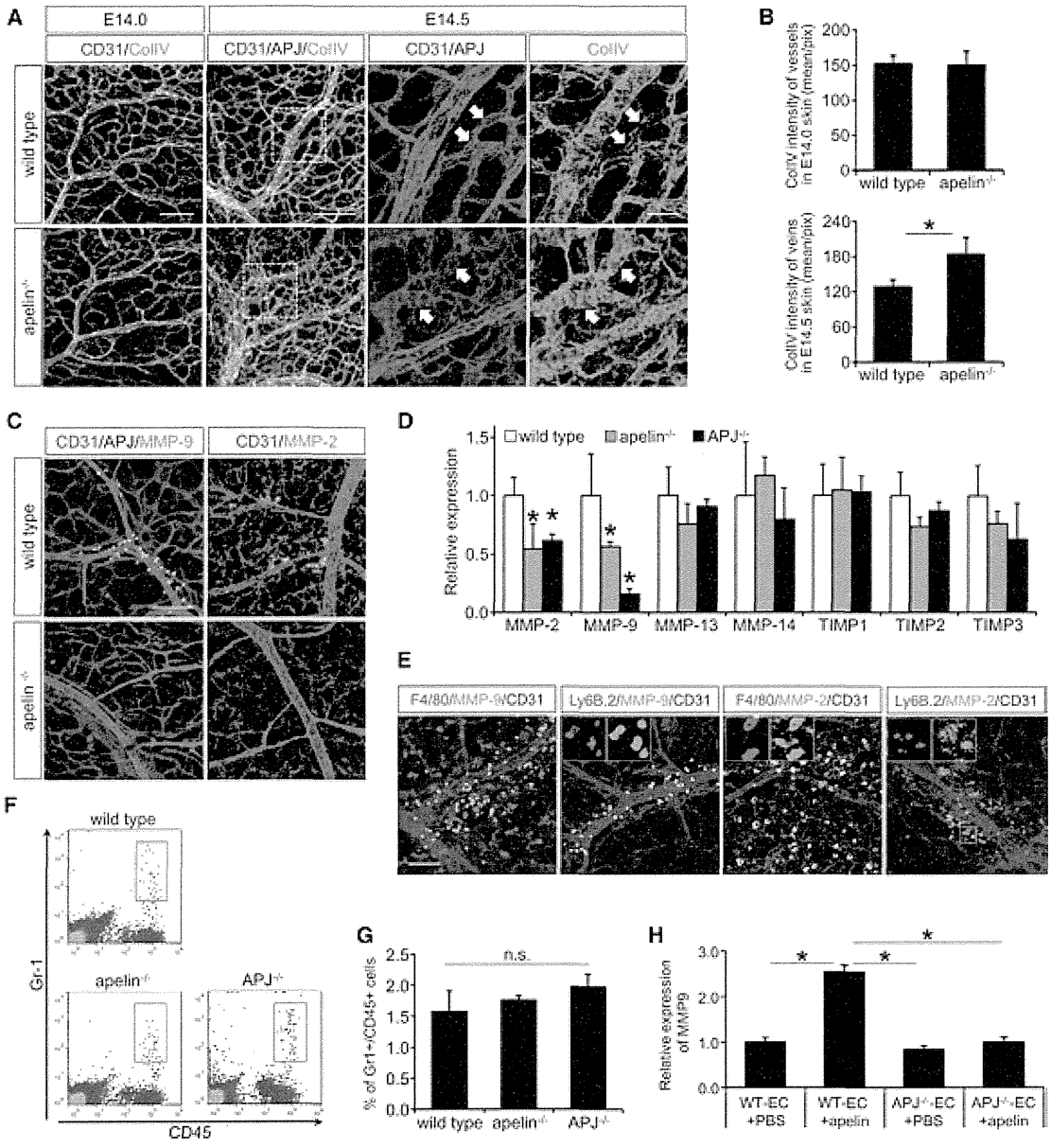

Figure 3. Venous Vascular Displacement Is Mediated by ECM Degradation

(A) Expression of collagen type IV (ColIV) (green) in $CD31^+$ (red) vessels of back skin from E14.0 embryos and in APJ^+ (blue) veins of E14.5 wild-type or *apelin*$^{-/-}$ embryos. The middle and right panels in E14.5 show a higher magnification of the areas indicated by the white dashed boxes where venous vascular displacement is induced. Note that attenuation of collagen type IV expression was observed in wild-type but not in *apelin*$^{-/-}$ mice (white arrows). The scale bars represent 200 μm (left) and 50 μm (middle and right).

(B) Quantitative evaluation of immunohistochemical staining for collagen type IV in the back skin of E15.5 WT or *apelin*$^{-/-}$ embryos. Data represent the means ± SD; n = 6 independent samples per group. *$p < 0.01$.

(C) Immunohistochemical analysis of MMP-9 and MMP-2 expression in the back skin of an E14.5 mouse embryo. Blood vessels were stained with anti-CD31 (red) and anti-APJ (blue) Abs. Note that MMP-9 or MMP-2 proteins (green) were present between the artery and the vein in wild-type but not in *apelin*$^{-/-}$ mice. The scale bar represents 100 μm.

(D) qRT-PCR analysis of mRNA for MMPs and tissue inhibitors of metalloproteinase (TIMPs) as indicated in E14.5 embryo back skin cells harvested from wild-type, *apelin*$^{-/-}$, or *APJ*$^{-/-}$ mice. Data represent the means ± SD; n = 5 independent cell lines per group. *$p < 0.01$.

(E) Immunohistochemical analysis of F4/80 (red)- or Ly6B.2 (red)-expressing cells with CD31 (blue) and MMP-9 (green) or MMP-2 (green) expression in the back skin of E14.5 mouse embryos. The insets in the upper left corners show the single staining of the areas indicated by the dashed boxes. The scale bar represents 100 μm.

(F) Representative flow cytometric plots of skin cells from E14.5 mouse embryos from wild-type, *apelin*$^{-/-}$, or *APJ*$^{-/-}$ mice. The $Gr1^+CD45^+$ neutrophil fraction is gated as a red box.

(legend continued on next page)